Cretaceous Research 154 (2024) 105738

Contents lists available at ScienceDirect

Cretaceous Research

journal homepage: www.elsevier.com/locate/CretRes

Exploring the ceratopsid growth record: A comprehensive osteohistological analysis of *Triceratops* (Ornithischia: Ceratopsidae) and its implications for growth and ontogeny

Jimmy de Rooij [a, b, *], Sybrand A.N. Lucassen [b, c], Charlotte Furer [b, c], Anne S. Schulp [a, b], P. Martin Sander [d, e]

[a] Faculty of Geosciences, Utrecht University, Princetonlaan 8A, 3584 CB Utrecht, the Netherlands
[b] Naturalis Biodiversity Center, Darwinweg 2, 2333 CR Leiden, the Netherlands
[c] Institute of Biology, Faculty of Science, Leiden University, Sylviusweg 72, 2333 BE Leiden, the Netherlands
[d] Section Paleontology, Institute of Geosciences, University of Bonn, Nussallee 8, 53115 Bonn, Germany
[e] Dinosaur Institute, Natural History Museum Los Angeles County, 900 Exposition Boulevard, CA 90007, Los Angeles, USA

ARTICLE INFO

Article history:
Received 14 April 2023
Received in revised form
25 September 2023
Accepted in revised form 2 October 2023
Available online 7 October 2023

Keywords:
Ceratopsian
Ontogeny
Skeletochronology
Bone remodelling
Histovariability

ABSTRACT

Ceratopsids represent one of the most iconic groups of non-avian dinosaurs. These large quadrupedal ornithischians are well-known for their bizarre cranial ornamentations, which are distinctive among different ceratopsids. However, only very little data exist on ceratopsid osteohistology and growth rates. Here, we present a detailed osteohistological analysis on *Triceratops horridus* preserved in a relatively large bonebed from the Lance Formation (eastern Wyoming, USA) as well as additional *Triceratops* cf. *prorsus* specimens from Canada. Deciphering the bone microstructure of this iconic dinosaur allows to better understand the growth and development of ceratopsids. The *Triceratops* limb elements show a distinct pattern of slower growing parallel-fibred and faster growing woven-parallel bone tissue that serves as basis for the definition of histologic ontogenetic stages (HOS). Lower (i.e., younger) HOS correspond to woven-parallel tissue while higher (i.e., older) HOS correspond to parallel-fibred tissue. The intraskeletal variation in histology is best explained through the Three-Front Model, indicating significant differences in cortical thickness between different limb bones. The *Triceratops* primary growth record is poorly expressed, and the few growth marks preserved show irregular spacing inconsistent with expected growth patterns. The HOS scheme provides seven stages that correspond to biological age classes and that show a correlation with body size. Our analysis suggests that the taxonomic ambiguity between *Torosaurus* and *Triceratops* cannot be solved based purely on histological data, but requires additional taphonomic, taxonomic and histological analyses. This study expands the current ceratopsian histological database and helps to better understand ceratopsid growth patterns.
© 2023 The Author(s). Published by Elsevier Ltd. This is an open access article under the CC BY license (http://creativecommons.org/licenses/by/4.0/).

1. Introduction

Bone histology informs about dinosaur growth patterns, age, longevity, (sexual) maturity, and metabolism (Horner et al., 1999; Sander, 2000; Chinsamy et al., 2012; Erickson, 2014; Waskow and Sander, 2014; Woodward et al., 2020). Almost all major dinosaur groups have received considerable attention in osteohistological analyses, including various species of sauropods (Sander, 2000; Klein and Sander, 2008; Sander et al., 2011; Waskow, 2019), theropods (Horner and Padian, 2004; Cullen et al., 2020), hadrosaurs (Horner et al., 2000; Słowiak et al., 2020) and thyreophorans such as stegosaurs (Redelstorff and Sander, 2009; Redelstorff et al., 2013; Waskow and Mateus, 2017) and ankylosaurs (Stein et al., 2013). However, to date horned dinosaurs have received little attention in osteohistological studies. Especially the osteohistology of more derived quadrupedal ceratopsids from North America remains vastly understudied, despite these comprising one of the most species-rich and well-sampled dinosaur groups.

The few histological analyses conducted on ceratopsians are restricted to more basal taxa such as *Psittacosaurus* (Erickson and

* Corresponding author. Faculty of Geosciences, Utrecht University, Princetonlaan 8A, 3584 CB Utrecht, the Netherlands.
E-mail address: jimmy.derooij@naturalis.nl (J. de Rooij).

https://doi.org/10.1016/j.cretres.2023.105738
0195-6671/© 2023 The Author(s). Published by Elsevier Ltd. This is an open access article under the CC BY license (http://creativecommons.org/licenses/by/4.0/).

Tumanova, 2000; Zhao et al., 2019; Skutschas et al., 2021), *Protoceratops* (Fostowicz-Frelik and Słowiak, 2018) and *Koreaceratops* (Baag and Lee, 2022). Ceratopsid histology has mostly been investigated in unpublished thesis projects and/or conference abstracts (including *Centrosaurus* (Lee, 2007), *Einiosaurus* (Reizner, 2010), *Kosmoceratops* (Levitt, 2013), *Pachyrhinosaurus* (Goldsmith, 2018; Vice, 2020), *Utahceratops* (Levitt, 2013), and *Triceratops* (Rooij, 2018)). These works hinted at differences in growth rate between more basal and more derived ceratopsids, mostly through histological markers such as remodelling patterns and cyclical growth marks. The limited body of published ceratopsid histology covers *Pachyrhinosaurus* (Erickson and Druckenmiller, 2011), *Avaceratops* (Hedrick et al., 2020), *Yehuecauhceratops* (Hedrick et al., 2020), as well as brief histological descriptions of *Medusaceratops* (Chiba et al., 2018) and *Spiclypeus* (Mallon et al., 2016). In addition, Horner and Lamm (2011) explored the histology of the *Triceratops* parietal frill, while Mallon et al. (2022) described femoral histology of *Torosaurus*. However, the results in these projects provided limited data on ceratopsian growth patterns and were often based on single – and fragmentary – elements. In fact, chasmosaurine and centrosaurine species are almost exclusively identified based on their cranial ornamentation, and limb elements suitable for histological sectioning have been described much less often (Chiba et al., 2018; Chinnery, 2004; Holmes and Ryan, 2013; Maidment and Barrett, 2011; Mallon et al., 2016; Mallon and Holmes, 2010; Scott et al., 2023). As a result, the ceratopsian histological record remains relatively unexplored, and our understanding of ceratopsid growth strategies is still limited.

Here we provide an in-depth osteohistological description of *Triceratops*, an iconic horned dinosaur from the Late Cretaceous of North America (Goodwin et al., 2006; Horner and Goodwin, 2006, 2008). The histological analysis is based on a multi-element approach across multiple individuals to visualize and understand their bone microstructure in as much detail as possible. Comparisons with other dinosaur taxa for which detailed histological data are available allow to better comprehend ceratopsid growth strategies and potential life history parameters.

2. Material and methods

2.1. Institutional abbreviations

CMN, Canadian Museum of Nature, Ottawa, Canada; RSM, Royal Saskatchewan Museum, Regina, Canada; RGM, Rijksmuseum voor Geologie en Mineralogie (now NBC, Naturalis Biodiversity Center, Leiden, the Netherlands).

2.2. Geological background

The majority of the material used in this study is part of a relatively large monodominant mass death assemblage preserving the remains of at least five individuals belonging to the genus *Triceratops* (see Rooij et al., 2022 for more details). The bonebed, named the 'Darnell *Triceratops* Bonebed' (DTB), occurs in eastern Wyoming, USA on the south-eastern flank of the Powder River Basin. It is situated in the upper Maastrichtian Lance Formation (Bartos et al., 2021) and – based on its closer proximity to the underlying Fox Hills Formation – dates back to c. 67 Mya. Its stratigraphic position as well as preliminary surveys on preserved cranial elements suggest that the preserved species pertains to *Triceratops horridus* (Bastiaans et al., 2016; Forster, 1996b; Scannella et al., 2014). A low-energy depositional environment combined with rapid burial resulted in overall excellent preservation of the fossil material (Kaskes et al., 2019; Rooij et al., 2022). However, subsequent crevasse splay events as evidenced by increase in lithogenic grain size resulted in reburial of the fossil elements and caused high degrees of disarticulation (Rooij et al., 2022). The DTB is characterized by a relatively large proportion of post-cranial elements including limb and girdle bones, ribs and vertebrae. For the limb bones in particular, it is clear that the material represents only larger individuals close to known maximum body size for *Triceratops*. Morphological distortion is limited, and the majority of the skeletal elements retain their original bone surface, providing for the first time excellent opportunities for histological sectioning of a relatively large group of *Triceratops*.

2.3. Specimen selection

Limb bones are the most suitable candidates in histological analyses based on their relatively simple (i.e., symmetrical) morphology and growth pattern, providing a representative image of the developmental history in studied sections (Sander, 2000). Additionally, limb bones provide the best suitable data source for body size reconstructions (Sander, 2000; Klein and Sander, 2008; Sander et al., 2011; Waskow and Sander, 2014). The femur and humerus are frequently studied in dinosaur histological research, as they possess the thickest cortex at midshaft preserving the most complete growth record (Sander, 2000). However, to explore the preservation of the histological record in different limb elements as thoroughly as possible, we selected all three autopodial and zeugopodial forelimb (radius, ulna, humerus) and hindlimb (fibula, tibia, femur) elements to study the *Triceratops* histology.

In addition to the bonebed material, we sampled an additional six *Triceratops* limb elements housed in various Canadian institutes in order to expand the coverage of ontogenetic ranges in our sampling strategy as much as possible. These include material housed in the collections of CMN and RSM. The Canadian specimens were not identified to the species level, but as they were all preserved in the Frenchman Formation, they most likely pertain to *Triceratops prorsus* (Tokaryk, 1986). As such, the complete dataset consists of both *Triceratops* species which could potentially introduce some degree of uncertainty when discussing the histological data. However, considering that the majority of the samples are from a single species and the ontogenetic range is relatively large, we do not expect appreciable offsets in histology as a result of taxonomic differences. Moreover, ceratopsids show a relatively conserved post-cranial skeleton (Chinnery, 2004) which is not expected to translate to significant differences in histology, especially for the two closely related *Triceratops* species which are distinguished based on mostly cranial characteristics (Forster, 1996a,b). Nevertheless, we incorporated both taxa in our histological analysis to provide additional context on potential histological and ontogenetic offsets related to taxonomic differences (see Section 4.7). The dataset is represented by a total of two radii, three ulnae, six humeri, four fibulae, six tibiae and four femora. Table 1 provides a complete list of all the sampled material and their details, and Fig. S2–5 shows photographs of all limb bones sampled for this study.

Additionally, it has been shown that sauropod dinosaurs may preserve a near-complete growth record in their ribs (Waskow and Sander, 2014; Waskow, 2019), but previous work on centrosaurine rib histology returned poorly preserved primary growth records (Hedrick et al., 2020). Thus, to further explore the preservation of the histological record in different skeletal elements, we sampled the axial skeleton of *Triceratops*, including three ribs and neural and transverse vertebral processes. Ribs and vertebrae were selected to cover a wide range of the *Triceratops* anatomy, and include a cervical vertebra, thoracic vertebra, an anteriorly positioned rib and posteriorly positioned rib (position reconstructed based on proximal bend in capitulum).

Table 1
List of specimens sampled and discussed in this study. Where applicable, these include details of the dimensions of the skeletal elements as well as assigned histologic ontogenetic stage (HOS). Percentage maximum lengths are calculated by comparing bone lengths to calculated bone proportions for each limb bone type, based on an associated specimen of *Triceratops horridus* (see Section 2.5 and Table S1 for details on calculation). Relative cortical thickness in the samples are calculated by dividing the measured cortical thickness by the length of the core sample. Cortical thickness equals the radius of the bone and was measured from the innermost medullary cavity to the bone surface using the CT scans in Supplements Fig. 1. Measurements with an asterisk (*) indicate reconstructed lengths of incomplete limb bones based on scaling and extrapolation from other well-preserved bones.

Collection ID	Species	Element	Side	Length (mm)	% Maximum length	Circumference at plane of sampling (mm)	Cortical thickness at sample site (mm)	Length of core sample (mm)	Portion cortical thickness in core sample	HOS
RGM.1394097	*Triceratops horridus*	Rib	–	–	–	–	–	–	–	–
RGM.1394098	*Triceratops horridus*	Rib	–	–	–	–	–	–	–	–
RGM.1394100	*Triceratops horridus*	Dorsal vertebra	–	–	–	–	–	–	–	–
RGM.1394101	*Triceratops horridus*	Cervical vertebra	–	–	–	–	–	–	–	–
RGM.1394102	*Triceratops horridus*	Humerus	Left	761	99	382	23	24	1.04	6
RGM.1394103	*Triceratops horridus*	Humerus	Right	651*	85	313	22	24	1.09	4
RSM P.2691	*Triceratops* cf. *prorsus*	Humerus	Left	205	27	89	4	18	>1.00	2
RSM P.3324.6.1	*Triceratops* cf. *prorsus*	Humerus	Left	550	72	–	–	8	<1.00	3
CMN 9533	*Triceratops* cf. *prorsus*	Humerus	Right	–	–	445	–	31	>1.00	6
RSM P.1163.9	*Triceratops* cf. *prorsus*	Humerus	Left	803	105	472	–	22	>1.00	7
RGM.1394104	*Triceratops horridus*	Radius	Left	482	110	219	17	24	1.41	6
RGM.1394105	*Triceratops horridus*	Radius	Right	462	106	212	13	13	1.00	7
RGM.1394106	*Triceratops horridus*	Ulna	Right	680	99	288	29	20	0.69	7
RGM.1394107	*Triceratops horridus*	Ulna	Right	649*	95	265	24	20	0.83	5
RSM P.2095	*Triceratops* sp.	Ulna	Left	613	90	290	–	19	<1.00	7
RGM.1394108	*Triceratops horridus*	Femur	Right	1125*	10	479	43	44	1.02	6
RGM.1394109	*Triceratops horridus*	Femur	Right	1039	93	469	38	38	1.00	4–5
RGM.1394110	*Triceratops horridus*	Femur	Left	1120	100	408	34	24	0.71	6
RGM.1394111	*Triceratops horridus*	Femur	Right	1004	90	429	37	37	1.00	4
RGM.1394112	*Triceratops horridus*	Tibia	Right	–	–	–	–	24	<1.00	5
RGM.1394113	*Triceratops horridus*	Tibia	Left	785	102	368	–	18	<1.00	6
RGM.1394114	*Triceratops horridus*	Tibia	Left	781	101	355	41	37	0.90	6
RGM.1394115	*Triceratops horridus*	Tibia	Right	783*	101	367	34	32	0.94	6
RGM.1394116	*Triceratops horridus*	Tibia	Right	740	96	331	38	23	0.61	5
RGM.1394117	*Triceratops horridus*	Tibia	Left	704	91	324	35	36	1.03	5
RGM.1394118	*Triceratops horridus*	Fibula	Left	645	86	163	15	21	1.40	5
RGM.1394119	*Triceratops horridus*	Fibula	Left	616	85	157	12	11	0.92	7
RGM.1394120	*Triceratops horridus*	Fibula	Right	637	88	157	10	10	1.00	6
CMN.57065	*Triceratops cf.* prorsus	Fibula	–	–	–	206	–	21	>1.00	7

2.4. Histological sampling strategy

Traditional histological sampling and thin-sectioning requires a complete cross-section of limb bones (Chinsamy and Raath, 1992; Stein and Sander, 2009). This approach severely compromises the original morphology of fossils and curators are thus understandably more reluctant to grant access, especially when considering unique and well-preserved material suitable for museum exhibitions. However, well-preserved fossils generally have equally well-preserved internal microstructure suitable for histology, and knowing more about the histology provides additional information to enrich museum exhibitions as well. To minimize the impact on the material, we opted for a different approach. The sampling strategy applied here combines the histological coring method (HCM, Sander, 2000; Stein and Sander, 2009) with medical CT scans (Fig. 1). CT imaging prior to sampling as best practice complements the HCM by revealing the ideal sampling location on each element. Identification of the most suitable sampling area on a specific bone is based on overall preservation such as fractures/cracks and diagenetic infill surrounding the mid-diaphysis (see Supplements for details on CT scans). Additionally, each sampling area was only considered if it was available in all bones of the same type. Following these two criteria helped determining standardized sampling locations for each limb bone type. CT cross-sections and sampling locations for each available (limb) bone are found in Fig. S1. Accordingly, this approach enables homologous sampling important for inter-bone comparisons (Sander, 2000; Woodward et al., 2014; Prondvai et al., 2018; Cullen et al., 2021) and provides access to the internal bone microstructure of unique material with minimal impact on its morphology.

The two ribs and vertebral processes were sampled without using CT scans as visual inspection yielded sufficient confidence on preservation and ideal sampling location. The axial skeletal elements were sampled following a transect from proximal to distal end (Fig. 1), yielding five samples for rib RGM.1394097, three samples for rib RGM.1394098, four samples for dorsal vertebra RGM.1394100 and three samples for cervical vertebra RGM.1394101. The rib sections did not cover the entire length of the rib, and the most distal sample reached approximately just over halfway of the total shaft length due to relatively poor preservation of rib elements (e.g., RGM.1394097, Fig. 1). Core samples were retrieved centrally between the medial and lateral area of the shaft, intersecting both the anterior and posterior cortical surface. In addition, we made a complete thin-section of rib RGM.1394121 just distally from the tuberculum–capitulum junction to compare the medial- and lateral-most areas with samples from the HCM (Fig. 1).

Thin-sections were prepared following standard methods (cf. Chinsamy and Raath, 1992; Lamm, 2013), where each sample was ground by hand until the desired thickness was reached. Sections were studied under normal transmitted and polarized transmitted light using a Leica DMR light microscope housed at Naturalis Biodiversity Center, the national natural history museum of the Netherlands. Photographs were taken using a Nikon DS-Ri2 digital microscope camera mounted on a Nikon Eclipse E600POL

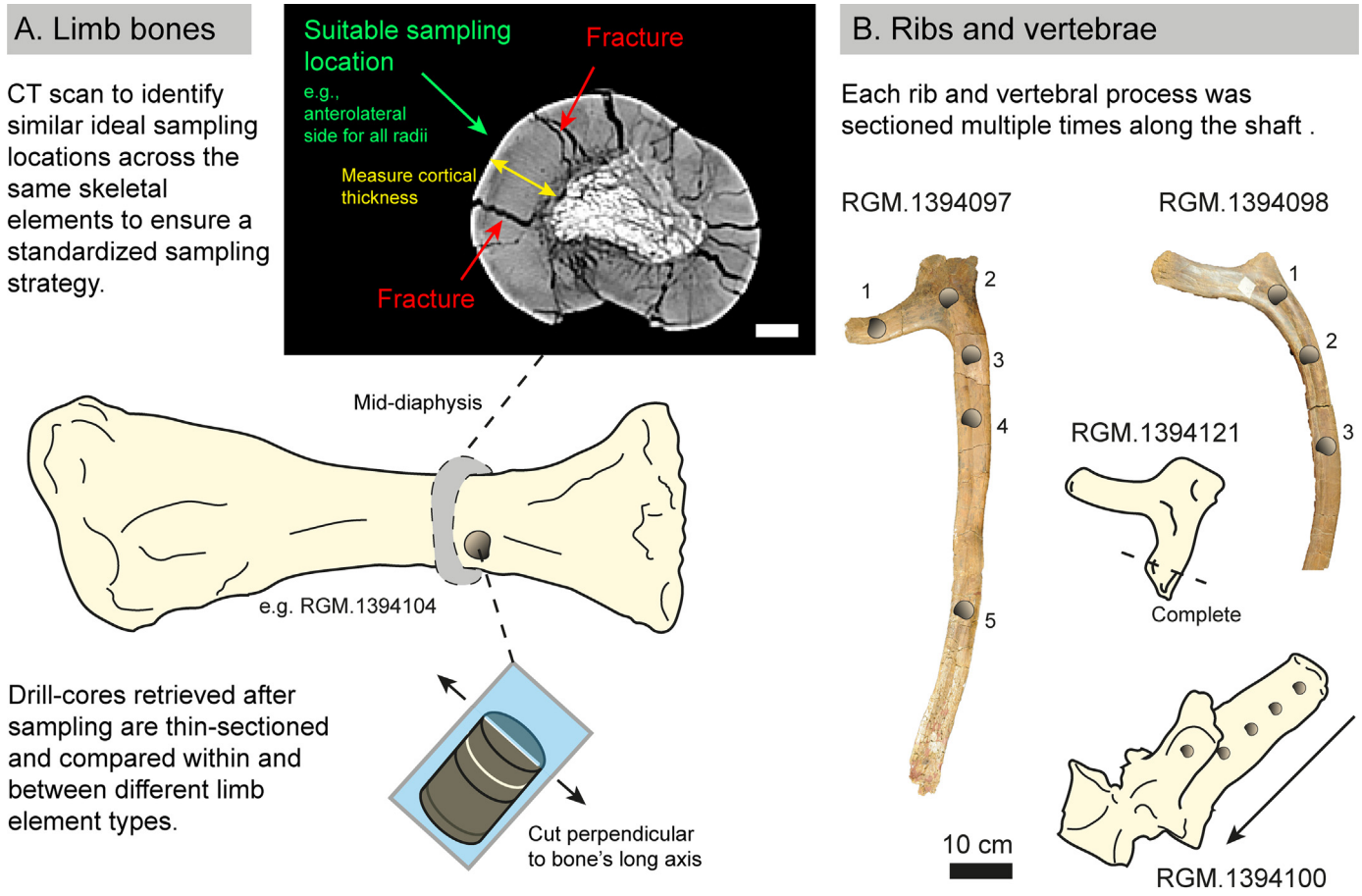

Fig. 1. Overview of the applied methodology for limb and axial bones. Scale bar in the CT image is 1 cm.

polarizing light microscope housed in the Dutch Gemmology Laboratory at Naturalis. Terminology for histological markers follows Buffrénil and Quilhac (2021).

2.5. Osteohistological analysis

In an effort to analyse the *Triceratops* histology beyond the description of basic histological markers, we focussed on additional methods to better constrain the growth patterns and age classes of the DTB *Triceratops*. First of all, we identified (annual) growth cycles in specific limb elements to evaluate the preservation of the primary growth record and potential for a skeletochronological analysis. Additionally, we applied the three-front model (Mitchell and Sander, 2014) to describe and better understand the observed histovariability between different types of limb elements. Although originally developed for sauropod dinosaurs, the three-front model can be applied to any histological description of the periosteal territory in amniotes (e.g., in plesiosaurs; Sander and Wintrich, 2021). The three-front model conceptualizes the observed patterns of cortical histology as the result of the interplay of three fronts. These simultaneously migrate from the centre of the bone outwards but differ in speed. Bone tissue is initially laid down by the apposition front (AF) which is followed by the Haversian substitution front (HSF), turning the primary tissue to secondary tissue. The HSF then is followed by the resorption front (RF) which turns compact tissue to cancellous tissue or an open medullary space (Mitchell and Sander, 2014).

The speed of the AF can be determined from histological indicators (e.g., parallel-fibred vs. woven bone, density and direction of vascular canals) but that of the HSF is considered constant, at least within a single low-level clade (Mitchell and Sander, 2014). For want of a method of speed determination of the HSF, constant speed is the most parsimonious assumption. The fact that the three-front model approach produced internally consistent results with its assumption of constant speed of the HSF (Mitchell and Sander, 2014) suggests that this assumption is reasonable. The speed of the RF is determined relative to the other two fronts. Note that the RF can overtake the HSF, resulting in a lack of remodelling, and that the HSF will overtake the AF when skeletal maturity is reached, resulting in a completely remodelled cortex (Mitchell and Sander, 2014).

Complementing the three-front model, we focussed on erecting histological ontogenetic stages (HOS, see Klein and Sander, 2008; Mitchell et al., 2017; Sander and Wintrich 2021) to establish a histological growth series for *Triceratops*. HOS were formulated based on the prevalence of different tissue types in any given section. Tissue types of use in defining HOS were described based mostly on characteristics of the bone matrix organisation, vascularity (primary osteons and simple vascular canals) and bone remodelling patterns.

In order to more accurately constrain the histological results of the skeletochronological analysis, the application of the three-front model and HOS, we calculated the percentage total lengths compared to estimated maximum lengths for each long bone

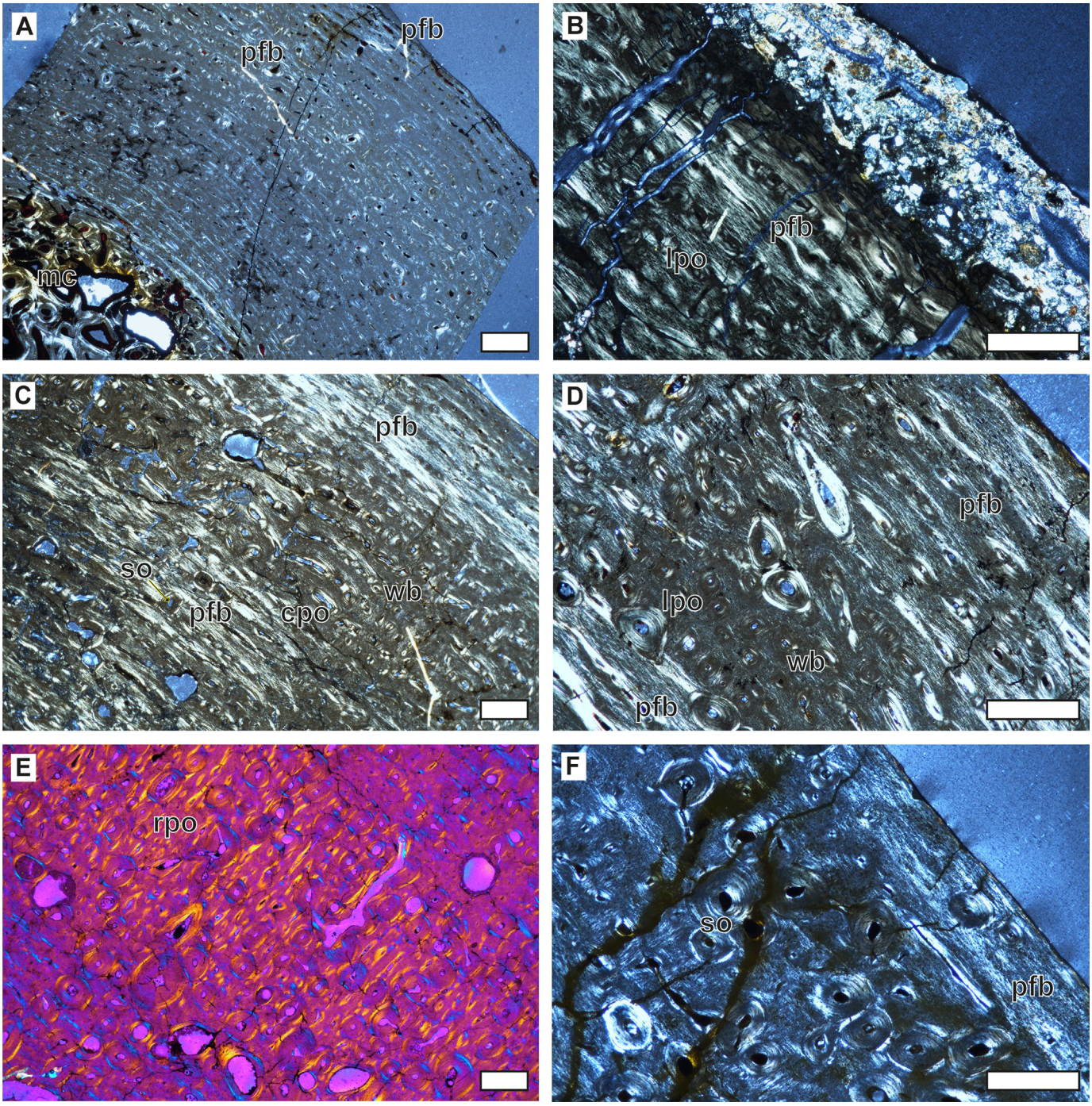

Fig. 2. Overview of *Triceratops* humerus histology. Bone surfaces are towards the upper right corner for all images. All images are in cross-polarized light, and Fig. 2E is with lambda-filter. A. Juvenile humerus RSM P.2691 (205 mm) showing a well-vascularized woven-parallel bone complex. The lower and upper parts of the cortex contain circumferential primary osteons while the mid-cortex represents a more conspicuous zone of longitudinal primary osteons. Overall, the lamellar centripetal infill of primary osteons is relatively weak. B. Humerus of early/late juvenile RSM P.3324.6.1 (550 mm) containing large zones of parallel-fibred bone tissue near the bone surface. There is a layer of sediment adhering to the bone surface. The primary osteons are relatively small and inconspicuous but are embedded in the parallel-fibred primary bone. C. Sub-adult humerus RGM.1394103 (651 mm) showing better defined zones of parallel-fibred and woven bone. Secondary osteons appear already closer to the bone surface. D. Adult humerus RGM.1394102 (761 mm) with larger zones of parallel-fibred bone and more advanced remodelling front. There are still randomly distributed areas of woven bone containing small longitudinal primary osteons. E. Same element as in D, but the upper mid-cortex showing a zone of radial woven-parallel bone tissue. F. Adult humerus CMN 9533 with increasing amounts of secondary osteons. All scale bars are 500 μm. cpo, circumferential primary osteon; lpo, longitudinal primary osteon; mc, medullary cavity; pfb, parallel-fibred bone; rpo, radial primary osteons; so, secondary osteon; wb, woven bone.

(Table S1). First, we calculated other limb bone to femur ratios for each limb bone based on the associated *Triceratops horridus* skeleton RGM.1332500 housed at Naturalis Biodiversity Center, the Netherlands. While a detailed taphonomic description is outside the scope of this contribution and currently in preparation, RGM.1332500 preserves associated stylopodia and zeugopodia as suggested by the uniform preservation and relative association of the fossilised bones (see Fig. S1 for the bonemap). Moreover, the lack of any duplicate

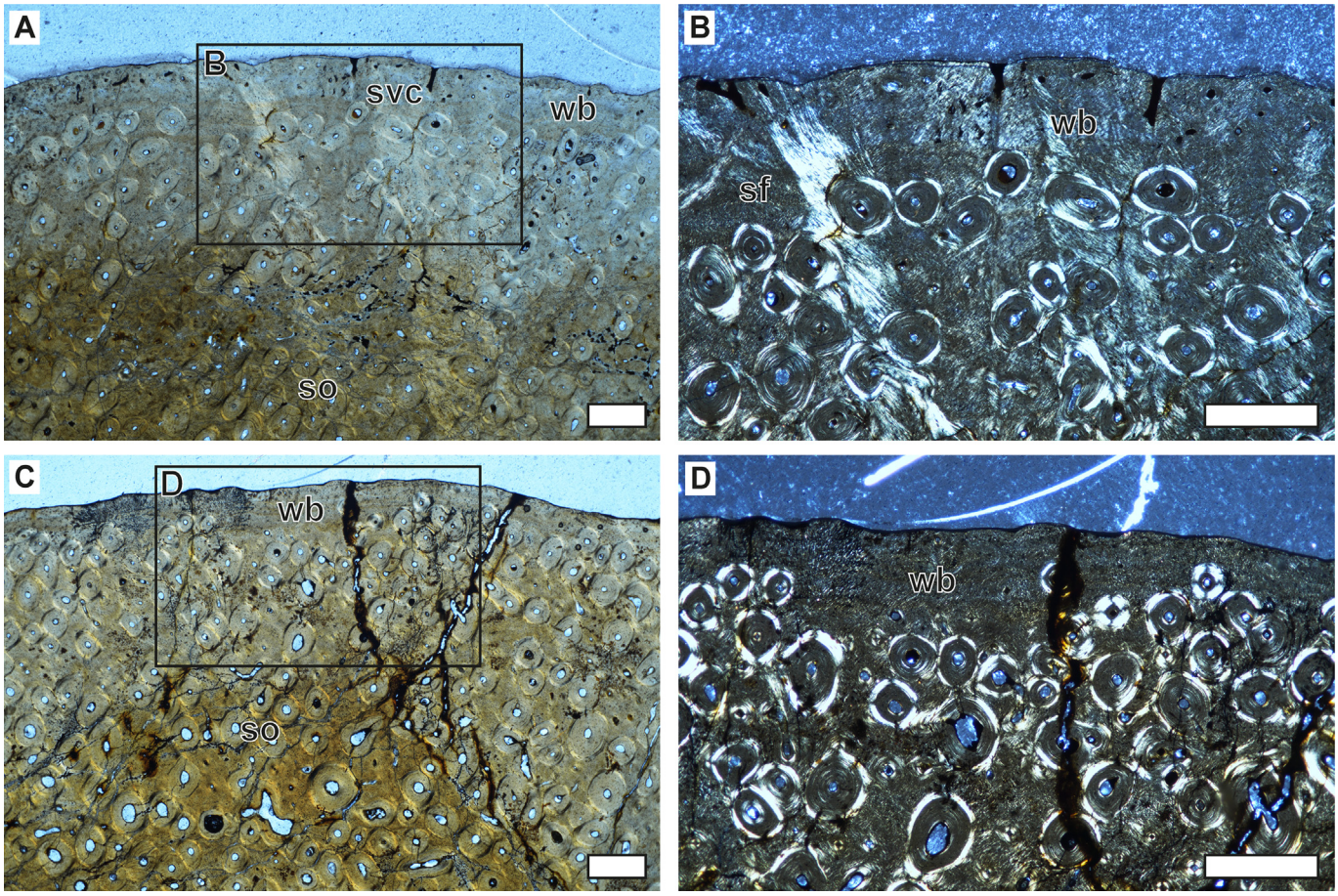

Fig. 3. Overview of *Triceratops* radius histology. Bone surfaces are towards the top of the images. A. Sub-adult radius RGM.1394104 (482 mm) showing woven primary bone in plane-polarized light. Primary osteons are small and inconspicuous, but the bone surface contains numerous simple vascular canals that open up at the bone surface. Bone remodelling is advanced, and only the periosteum remains devoid of secondary osteons. B. Close-up of the same element in cross-polarized light. Sharpey's fibres become more visible. C. Adult radius RGM.1394105 (462 mm) showing woven bone with increased amounts of remodelling in plane-polarized light. This radius does not contain simple vascular canals near the bone surface. D. Close-up of the same element in cross-polarized light. The small longitudinal primary osteons become better visible between the larger secondary osteons. All scale bars are 500 μm. sf, Sharpey's fibres; svc, simple vascular canals; so, secondary osteon; wb, woven bone.

elements as well as the presence of a narrow intraskeletal size range suggests that RGM.1332500 allows for accurate cross scaling of the studied bones, at least for the want of published measurements of associated skeletons. We acquired limb-to-femur ratios for all limb elements based on RGM.1332500, and applied this value to the largest femur available in this study, RGM.1394110 (Fig. S4). This allowed us to obtain a reliable estimate of *Triceratops* limb bones of potentially maximum size. Measurements of the studied bones were then divided by the corresponding calculated maximum size to obtain percentage maximum size estimates of each long bone (Table 1).

To compare the results of the histologic ontogenetic stages between *T. horridus, T. prorsus* and *Torosaurus* (see section 4.7), we calculated values for bone circumference normalized to associated femur circumference. We opted for this approach as the *Torosaurus* specimen was too fragmentary for length measurements leaving circumference as the most ideal proxy for body size (Mallon et al., 2022). We first calculated other limb bone to femur ratios for circumference measurements using RGM.1332500, and then applied the acquired ratios to calculate normalized circumference values for each sampled humerus, tibia and femur. This allowed us to visualize the relationship between body size and histologic ontogenetic stages for all three taxa (Fig. 19).

3. Results

3.1. Humeri

The *Triceratops* humeri are represented by an ontogenetic series of small, medium-sized and large individuals (Table 1). Overall, histology of *Triceratops* humeri show large areas of parallel-fibred bone tissue, where it substitutes the woven bone in a mostly longitudinal woven-parallel complex (Fig. 2B, D). They show cyclical patterns of parallel-fibred bone and woven bone, in which the parallel-fibred bone becomes increasingly more dominant towards the bone surface (Fig. 2C). This cyclicity is more prominent in larger humeri (Fig. 2). The smallest humerus (RSM P.2691) shows woven-parallel bone tissue containing a mixture of predominantly circumferential and longitudinal canals (Fig. 2A), while the second smallest humerus (RSM P.3324.6.1) already has shifted to clear parallel-fibred bone tissue near the bone surface (Fig. 2B). Among the larger humeri, the deeper cortex shows larger areas of woven-parallel bone tissue, but this quickly grades inwards into Haversian bone, and the primary tissue towards the bone surface shows an increase in bone tissue organisation (Fig. 2C). Nevertheless, the periosteal surface still contains patches of organized and

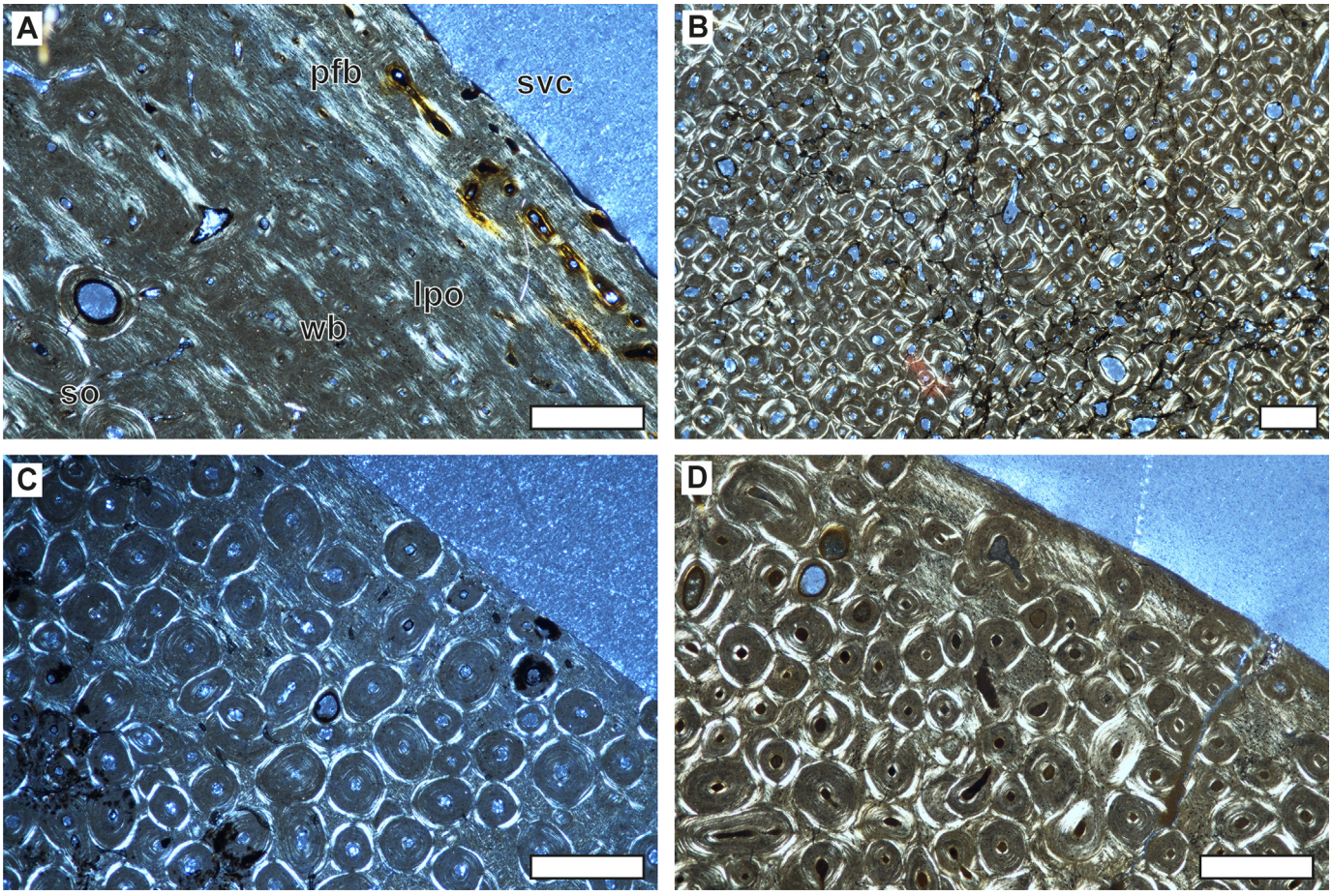

Fig. 4. Overview of *Triceratops* ulna histology. Bone surfaces are towards the upper right corner in all images. All images are in cross-polarized light. A. Sub-adult ulna RGM.1394107 (649 mm) showing primarily woven bone with a bone surface of slightly more parallel-fibred bone tissue. The periosteum contains simple vascular canals that occasionally open up to the bone surface. Primary osteons are exclusively longitudinal. Bone remodelling is advancing towards the bone surface. B. Mid-cortex of the same element showing dense Haversian tissue. C. Adult ulna RGM.1394106 (680 mm) with only little preserved primary bone due to overprinting of secondary osteons. The primary tissue shows a mix of woven and more organized patches of bone. D. Adult ulna P.2095 (613 mm) with the highest rates of bone remodelling containing multiple generations of secondary osteons near the bone surface. The bone surface seems more organized than woven bone. All scale bars are 500 μm. lpo, longitudinal primary osteon; pfb, parallel-fibred bone; so, secondary osteon; svc, simple vascular canals; wb, woven bone.

unorganized bone matrix. The predominant vascularity is characterized by longitudinal primary osteons accompanied by small amounts of randomly distributed circumferential osteons (with poorly defined laminae). However, the longitudinal osteons are relatively small, and are almost always positioned in circular rows parallel to the bone surface. These highly organized closely spaced longitudinal canals may resemble circumferential canals at lower magnification, thus the primary bone sometimes appears laminated (Fig. 2C).

Vascularity follows the alternating patterns in bone tissue organisation, with parallel-fibred bone containing relatively fewer primary osteons than woven bone. The smallest humerus is significantly more vascularized than larger humeri (Fig. 2D). However, the primary bone still shows occasional alternating cycles of longitudinal and circumferential vascularisation, as well as slight changes in bone tissue organisation, similar as in larger humeri. One humerus (RGM.1394103) has simple reticular vascular canals embedded in woven-parallel bone tissue that open at the bone surface, whereas the periosteal surface of larger humeri is underlain by a thin layer of poorly vascularized parallel-fibred bone tissue (Fig. 2F). This most likely represents an incipient external fundamental system (EFS), and one humerus preserves inconspicuous lines of arrested growth (LAGs) (RGM.1394102). Otherwise, LAGs are not visible in plane- and cross-polarized light in the other humeri. Approximately halfway through the bone cortex, humerus RGM.1394102 shows an area of radial vascularisation with thin vascular canals that runs along the complete width of the thin-section, which is not observed in other humeri (Fig. 2E).

Bone remodelling is evident in all but the two smallest humeri. In all but the largest humeri that show bone remodelling, there is still primary bone tissue preserved towards the bone surface, and dense Haversian bone is limited to only the deepest half of the cortex closer to the medullary cavity. The secondary osteons closer to the bone surface are less randomly distributed, but occasionally are aligned in circular rows parallel to the bone surface. More extensive remodelling in the form of resorption cavities is limited to the lower half of the bone cortex in larger humeri (Fig. 2F). Osteocyte density is uniform across the primary bone, but flattened osteocytes occur near the bone surface as well as in zones of parallel-fibred bone, especially in larger humeri. Besides the random occurrences of alternating cycles containing parallel-fibred and woven bone, and corresponding cyclical shifts in vascular patterns, growth lines occur sporadically and inconspicuously in all studied humeri leaving a poor skeletochronological growth record.

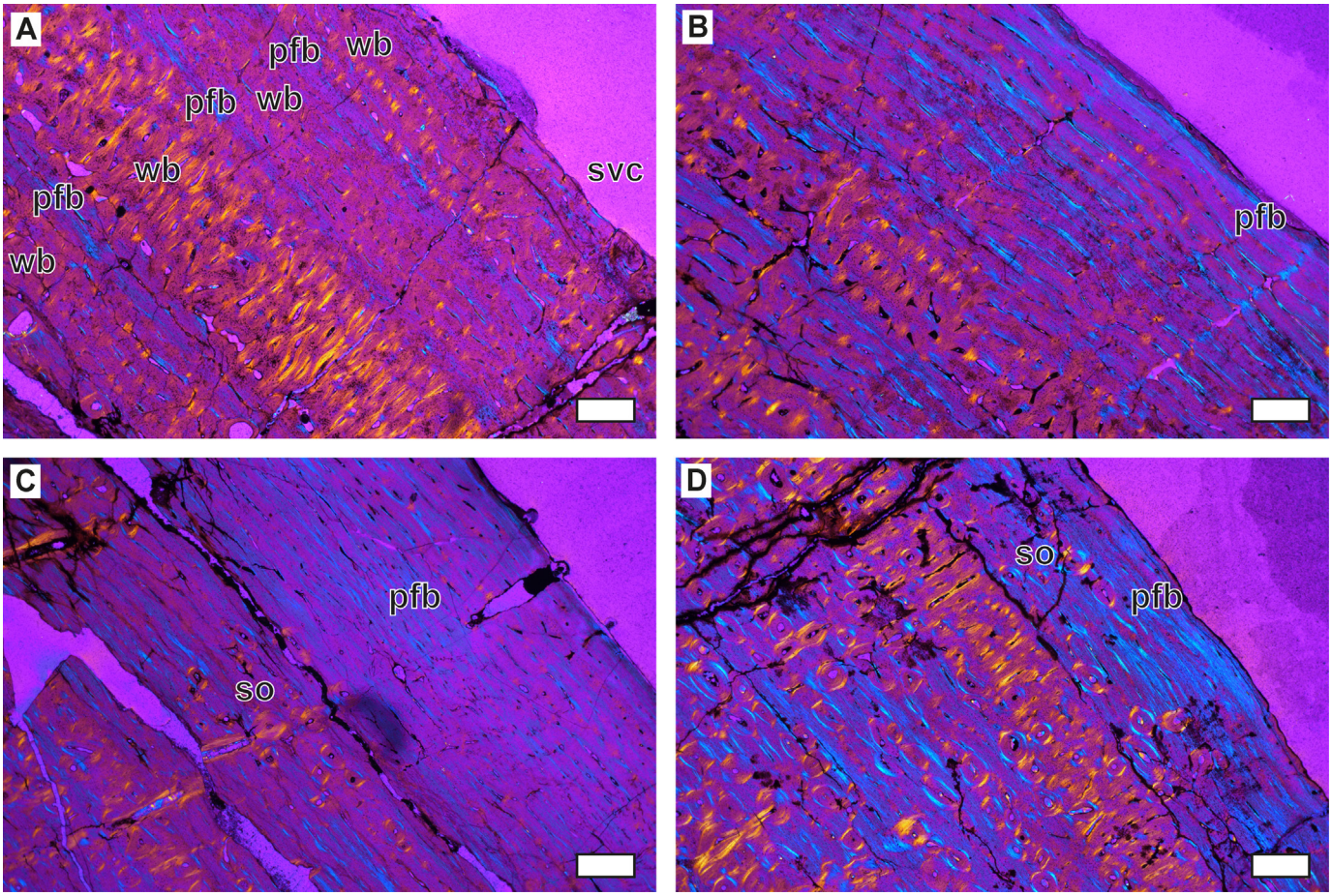

Fig. 5. Overview of *Triceratops* femur histology. Bone surfaces are towards the upper right corner for all images. All images are in cross-polarized light with lambda filter. A. Sub-adult femur RGM.1394109 (1070 mm) showing distinct zones of parallel-fibred and woven bone towards the bone surface. The parallel-fibred zones are represented by the thin blue birefringent lines. Vascular organisation is variable in each zone of woven bone, containing a mix of longitudinal, circumferential, radial and reticular primary osteons. The bone surface contains simple vascular canals. B. Sub-adult femur RGM.1394111 (1020 mm) with woven primary tissue that grades into parallel-fibred bone towards the bone surface. Vascularity is predominantly circumferential, and the lamellar infill of the primary osteons are very clear. C. Adult femur RGM.1394108 with relatively high portions of parallel-fibred bone and overall lower vascular density. Primary osteons are predominantly circumferential and longitudinal in circular rows. Secondary osteons are advancing towards the bone surface. D. Adult femur RGM.1394110 (1120 mm) showing large areas of parallel-fibred bone close to the bone surface and high rates of bone remodelling. All scale bars are 500 μm. pfb, parallel-fibred bone; so, secondary osteon; svc, simple vascular canals; wb, woven bone.

3.2. Radii

The two radii sampled (RGM.1394104, 482 mm and RGM.1394105, 462 mm) have mostly matching histological patterns and are approximately the same size, but show some differences in age-related histological markers. The radii mostly show longitudinal woven-parallel bone tissue based on their isotropic primary bone tissue. Vascularity is characterized by relatively small simple vascular canals as well as longitudinal primary osteons. Both radii lack primary osteons at the outer bone surface, but radius RGM.1394104 shows sporadic vascular canals lacking lamellar bone opening up to the bone surface (Fig. 3B). Radius RGM.1394105 shows nearly avascular bone tissue near the periosteum, but this is a relatively thin layer (Fig. 3D). Secondary remodelling is extensive in both radii, but markedly higher in radius RGM.1394105 (Fig. 3C, D). Nevertheless, secondary osteons do not reach the outermost part of the cortex but stay just below the bone surface. Primary bone tissue can still be observed between the secondary osteons all the way to the deepest cortex, where the onset of dense Haversian bone was just beginning. Larger resorption cavities lined with lamellar bone are limited to the deep cortex. Both radii show relatively high amounts of larger plump/rounded osteocytes uniformly distributed throughout the primary bone tissue, corroborating the presence of a predominantly woven-fibred bone matrix. Cyclical growth marks are absent throughout the cortex of both radii.

3.3. Ulnae

Similar to the radii, the three studied ulnae are fairly close in length and show the same histological characters, but differ in their age-related markers. Almost all of the primary bone is overprinted by secondary osteons that quickly grade into dense Haversian tissue towards the deeper cortex, even in the smallest ulna (Fig. 4B). The interstitial primary bone tissue is predominantly woven-parallel with longitudinally oriented primary osteons, similar to the radii. The primary osteons as well as the simple vascular canals are relatively small and in low abundance. Simple canals are mainly limited to the bone surface, but may occur randomly dispersed throughout the primary bone. The bone tissue near the periosteal surface changes to more parallel-fibred bone tissue, but still retains abundant primary osteons. In ulna RGM.1394107, this parallel-fibred bone tissue is also characterised by numerous simple vascular canals that occasionally open to the bone surface, as well as small numbers of primary osteons (Fig. 4A). These canals are longitudinal but may show anastomosing canals connecting to

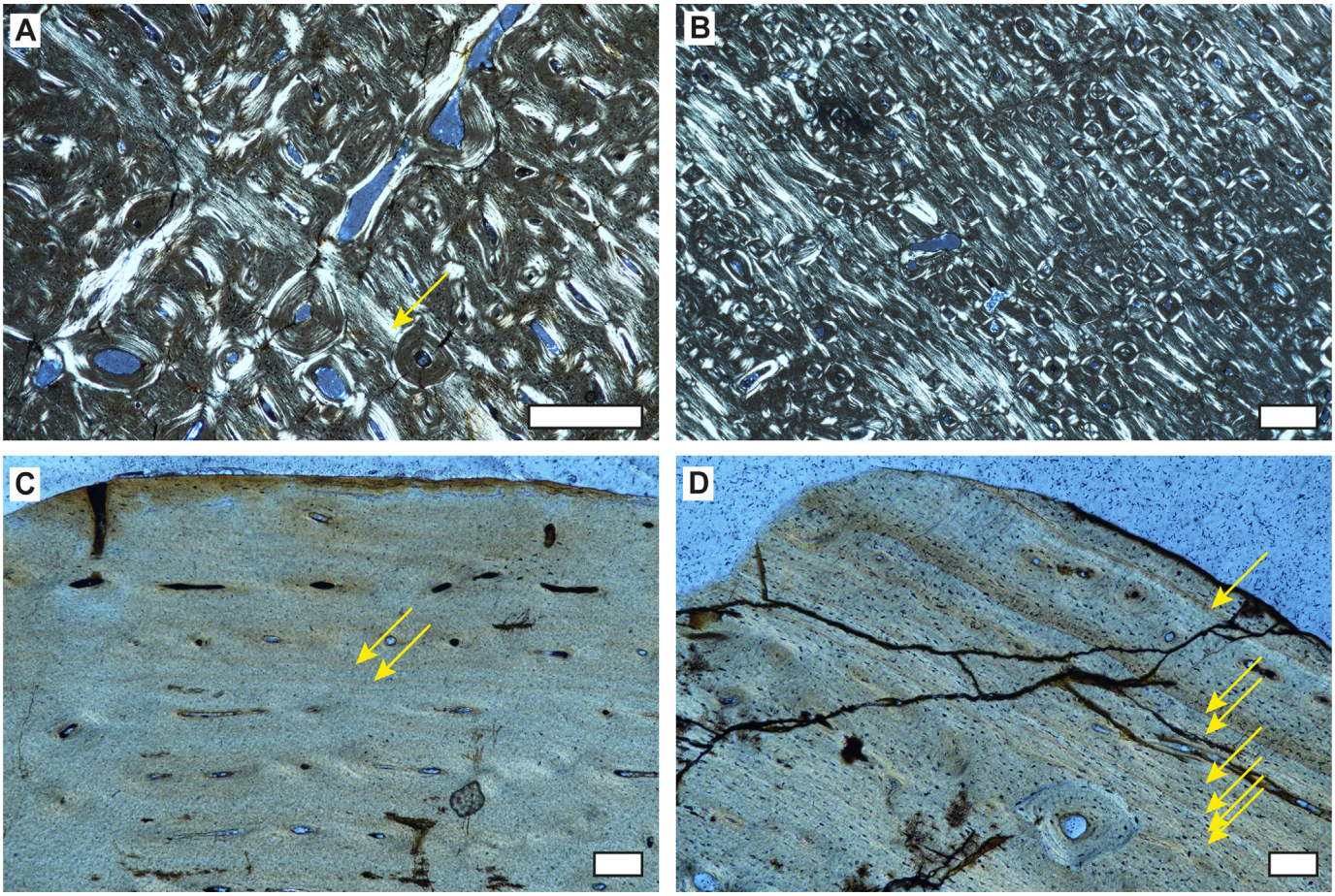

Fig. 6. Overview of cyclical patterns in *Triceratops* femora. Bone surface is towards the top and upper right corner. A. Arrow indicating lines/zones of parallel-fibred bone in the mid-cortex of sub-adult femur RGM.1394109 (1070 mm) in cross-polarized light. These zones were counted for age estimations. Note the overlapping secondary osteons overprinting the primary tissue. B. Alternating zones of parallel-fibred and woven bone in adult femur RGM.1394108 as indicated by the marked changes in birefringence in cross-polarized light. C. Arrows indicating two closely spaced growth lines (LAGS) near the bone surface of the same femur in plane-polarized light. D. Arrows indicating seven closely spaced growth lines in the bone surface of adult femur RGM.1394110 (1120 mm). Scale bar for A and B is 500 μm and for C and D is 100 μm.

neighbouring canals. Ulna RGM.1394106 shows avascular parallel-fibred bone just beneath the bone surface which is overprinted with secondary osteons. This indicates a distinctive decrease in the bone apposition front (AF) which is about to be overtaken by the Haversian substitution front (HSF) (Fig. 4C). Ulna P.2095 shows a more advanced degree of remodelling with multiple generations of overlapping secondary osteons close to the bone surface (Fig. 4D), i.e., the Haversian substitution front has progressed further than in RGM.1394106. Nevertheless, even the most heavily remodelled ulnae still preserve areas of primary (and active) bone. Osteocyte shape and abundance are uniform across the entire primary bone cortex for all three ulnae, with only minor local differences in shape and size. None of the sections show clear resorption cavities, even in the dense Haversian bone of the deep cortex. However, we do note that the ulnae preserve the least amount of primary bone as determined from the CT images, and that the deep cortical bone is not represented here (Table 1.). The ulnae do not show any growth marks.

3.4. Femora

The four studied *Triceratops* femora represent relatively large individuals, but differ in their onset and pattern of specific histological markers. The majority of the primary bone tissue of all femora shows variations of parallel-fibred and woven tissue in a laminar woven-parallel complex, in which the vascularity is mainly characterized by small longitudinal primary osteons in circular rows mixed in with fewer amounts of circumferential canals. These variations in bone tissue type are sequential, and all femora show alternating layers of parallel-fibred and woven bone – a recurring phenomenon in the larger *Triceratops* limb elements studied here (Fig. 5A). However, these cycles are mainly restricted to the outer cortex, and these growth cycles quickly disappear towards the medullary cavity. Nevertheless, the most pronounced differences between the femora are observed in the primary bone near the bone surface, in the extent of these alternating layers. Two femora (RGM.1394109 and RGM.1394111) contain significantly more areas of highly vascularized woven bone separated by thick layers of poorly vascularized parallel-fibred bone (Fig. 5A, B). Other femora (RGM.1394108 and RGM.1394110) show contrasting patterns, with markedly thicker layers of parallel-fibred bone tissue separated by thinner layers of more vascularized woven bone (Fig. 5C, D). Two femora (RGM.1394109 and RGM.1394110) also deposited radial primary osteons, but show otherwise contrasting primary tissue (Fig. 5A, D).

Osteocyte shape and density correlate with bone tissue organisation. Parallel-fibred bone contains lower densities of mostly flattened osteocytes, while woven bone shows higher densities of mainly plumb and rounded osteocytes with clear canaliculi. Bone remodelling is extensive in all femora, but even the most remodelled elements still preserve large portions of primary bone (Fig. 5D). The mid- to deep cortex of all femora is almost completely

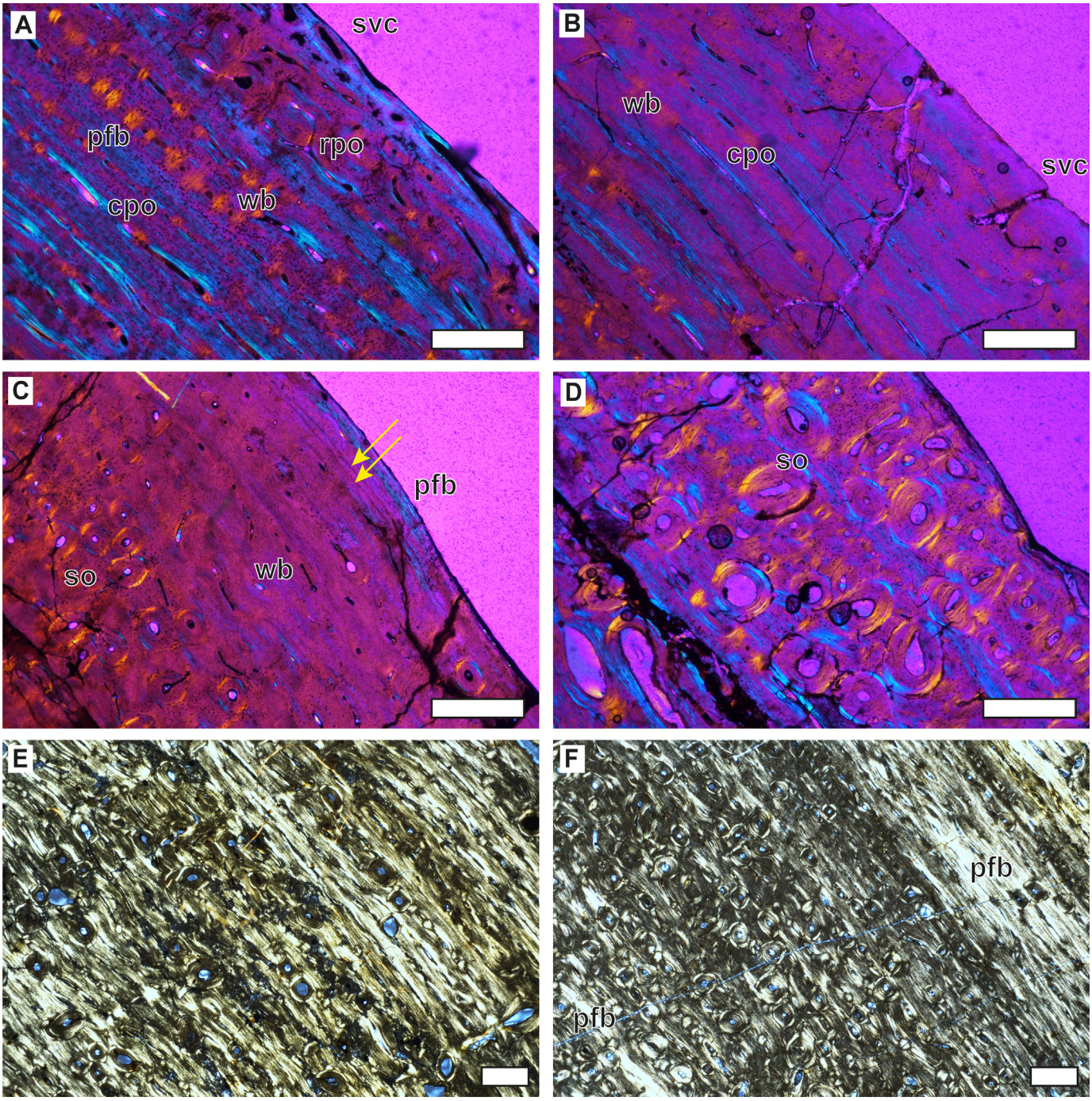

Fig. 7. Overview of *Triceratops* tibia histology. Bone surfaces are towards the upper right corner for all images. All images are in cross-polarized light. A–D are taken with lambda filter. A. Sub-adult tibia RGM.1394117 (704 mm) showing large areas of woven bone and inconspicuous layers of parallel-fibred tissue. The predominant vascularity is circumferential, but there are longitudinal primary osteons mixed in (highly birefringent). Close to the bone surface is an area of reticular and oblique primary osteons and simple vascular canals. B. Sub-adult tibia RGM.1394116 (740 mm) with large area of circumferential woven-parallel bone tissue. Some of the laminar organisation is due to the longitudinal canals oriented in circular rows (compare with A). There are some vascular canals that open up at the bone surface. C. Adult tibia RGM.1394114 (781 mm) showing woven bone and a parallel-fibred bone surface. Overall, vascular density is lower and secondary osteons become more pronounced closer to the bone surface. The arrows indicate two LAGs. D. Adult tibia RGM.1394113 (785 mm) with advanced bone remodelling and few visible longitudinal primary osteons in the primary bone. E. The mid-cortex of sub-adult tibia RGM.1394117 showing continuous zones of parallel-fibred bone matrix. There is some inconspicuous layering, but overall zones are poorly defined. F. The mid-cortex of adult tibia RGM.1394115 showing better defined layers of parallel-fibred and woven bone matrix. All scale bars are 500 μm. cpo, circumferential primary osteon; pfb, parallel-fibred bone; rpo, reticular primary osteon; so, secondary osteon; svc, simple vascular canal; wb, woven bone.

remodelled into Haversian tissue. Based on CT images, all femur cores were sampled up to the medullary border, except for RGM.1394110. However, larger resorption cavities are limited to the deeper cortex, and do not occur in all of the studied femora. In addition to the cyclical alternations in bone tissue type (Fig. 6A, B), two of the studied femora also show growth lines close to the periosteum. Femur RGM.1394108 has two to three closely spaced growth lines (Fig. 6C) and the outermost cortex is poorly

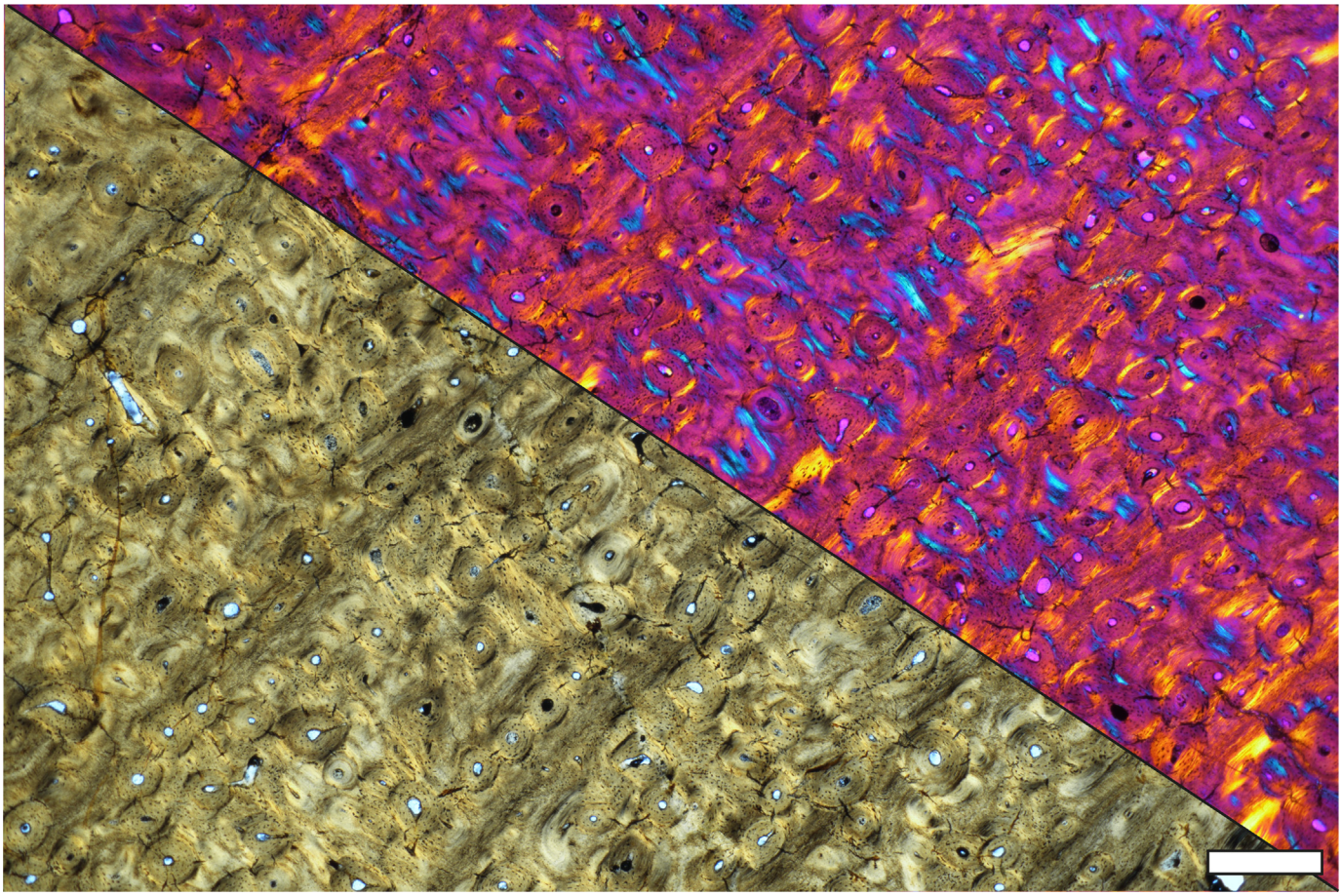

Fig. 8. The mid to deep cortex of adult tibia RGM.1394114 (781 mm) showing distinct layers of parallel-fibred and woven bone. The bone surface is towards the upper left corner. The lower left half is in plane-polarized light and the upper right half is in cross-polarized light with lambda filter. The zones are of parallel-fibred bone are dark/black in plane-polarized light and orange in birefringent cross-polarized light. Despite the numerous secondary osteons, this tibia preserves a clear primary growth record. Scale bar is 500 μm.

vascularized. We interpret this feature as an incipient external fundamental system (EFS). Femur RGM.1394110, on the other hand shows a better defined EFS, consisting of up to seven growth lines which become increasingly more closely spaced towards the bone surface (Fig. 6D). Curiously, the bone matrix deposited with the LAGs does not show a typical lamellar organisation but still contains a mixture of woven and parallel-fibred bone.

3.5. Tibiae

The six *Triceratops* tibiae studied here are all relatively close in size and represent large individuals, but they show distinct differences in histology (Fig. 7). All tibiae have primary bone tissue displaying a mix of parallel-fibred and woven bone, in which the two bone matrix types occur in alternating layers. The increase in parallel-fibred bone follows a simultaneous decrease of woven bone towards the bone surface, but the timing and preservation of this change in bone tissue ratio differs between tibiae. Vascular organisation of the primary tissue is almost exclusively characterized by small longitudinal primary osteons aligned in circular rows parallel to the bone surface, with occasional anastomosing canals (Fig. 7C). However, one tibia (RGM.1394116) contains predominantly circumferential primary osteons except near the periosteal surface (Fig. 7A). Tibia RGM.1394117 shows a mostly laminar organisation but has some reticular and oblique primary osteons near the bone surface (Fig. 7B). The degree of vascularity follows the same alternating pattern as the bone matrix organisation, resulting in layers of either poorly vascularized parallel-fibred bone or well-vascularized woven bone (Figs. 7A and 8). Based on Fig. 8, these are interpreted as cyclical growth marks. However, these cyclical growth marks are not observed as clearly in all tibiae, and only RGM.1394114 preserves a considerable growth record (Figs. 7E, F; 8).

Similarly, osteocyte abundance and morphology show sequential differences in these alternating layers of parallel-fibred and woven bone. Osteocytes in parallel-fibred bone are mostly flattened and occur at a lower density, while the woven-fibred bone matrix has denser groupings of plump osteocytes. Other forms of cyclicity such as growth lines are observed only in the three largest tibiae in which up to two growth lines have been deposited just beneath the periosteal surface (Fig. 7C). These growth lines are preceded by small areas of parallel-fibred bone tissue.

Bone remodelling is evident in all studied tibiae, but the overall density of secondary osteons differs significantly among all elements. In smaller tibiae, the HSF is less advanced and the cortex shows lesser degrees of bone remodelling and preserves considerable amounts of original primary bone near the bone surface, while larger tibiae already form secondary osteons near the periosteal surface and contain dense Haversian tissue in the deeper cortex (Fig. 7D). However, overall the remodelling pattern is diffuse, and primary bone may still be observed in deeper areas. Larger resorption cavities are extremely limited in all tibiae. While not all tibiae were sampled up to the medullary border as indicated by the CT images, the available cores that do represent a transect of the complete cortex also developed limited amounts of resorption cavities.

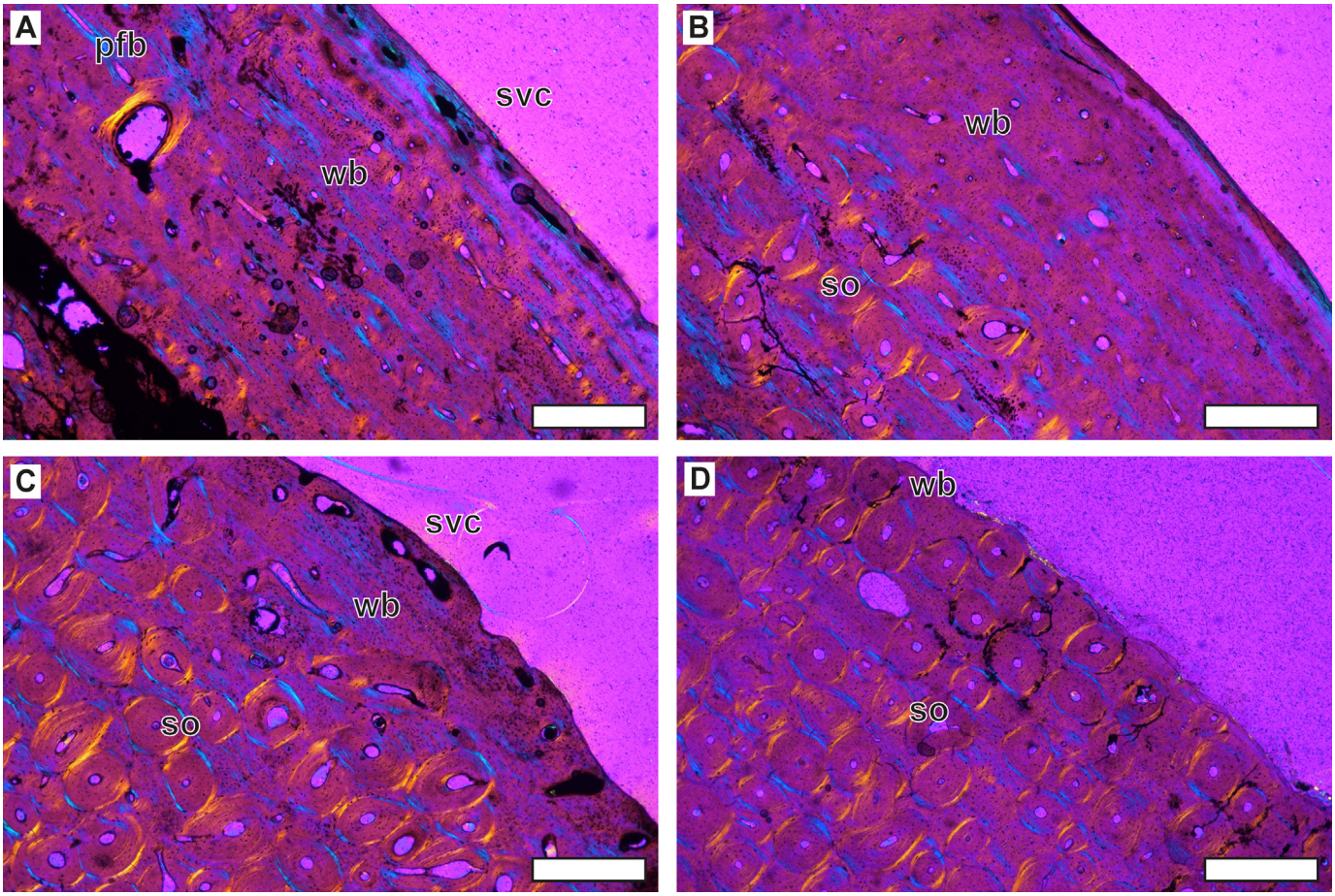

Fig. 9. Overview of *Triceratops* fibula histology. All images are in cross-polarized light with lambda filter. Bone surface are towards the upper right corner of all images. A. Sub-adult fibula RGM.1394118 (645 mm) showing woven bone with random patches of parallel-fibred bone. Vascular density is high with mainly laminar woven-parallel bone deposited with circumferential primary osteons as well as circular oriented longitudinal ones. Bone surface contains simple vascular canals. B. Sub-adult fibula RGM.1394120 (637 mm) with woven bone and small patches of parallel-fibred bone. Vascular density is relatively lower than RGM.1394118, and bone remodelling is more advanced. C. Adult fibula RGM.1394119 (616 mm) with high degree of bone remodelling and low vascular density in the primary tissue. Nevertheless, the primary bone is primarily woven, and the bone surface still contains numerous simple vascular canals. D. Adult fibula CMN.57065 in which the primary bone is almost entirely overprinted by secondary osteons. The preserved primary tissue is woven. All scale bars are 500 μm. pfb, parallel-fibred bone; so, secondary osteon; svc, simple vascular canal; wb, woven bone.

3.6. Fibulae

The four studied fibulae all represent relatively large individuals. Overall, the HSF has advanced close to the outer bone surface in all fibulae. Accordingly, bone remodelling is extremely high and they only preserve a relatively small amount of primary bone. This primary bone tissue is described as a woven-parallel complex with woven-fibred bone and small areas of parallel-fibred bone matrices (Fig. 9). In general, the vascular organisation of the primary bone is limited to small longitudinal primary osteons (Fig. 9A, B). In all fibulae, the vascular canals are relatively well-organized parallel to the bone surface. As with other studied *Triceratops* limb bones, the layers of parallel-fibred bone become thicker towards the bone surface. All fibulae show weakly expressed alternating zones of parallel-fibred tissue in their outer bone surface, but there is no clear pattern.

Fibula RGM.1394118 and RGM.1394119 still show simple vascular canals that occasionally open to the bone surface (Fig. 9A, C), but the two other fibulae possess a near avascular periosteal surface. There is a marked difference in the advancement of remodelling, where two fibulae (RGM.1394118 and RGM.1394120) have significantly fewer secondary osteons. Nevertheless, all fibulae have a diffuse remodelling pattern towards the bone surface and possess dense Haversian bone in the deep cortex, especially the largest fibula CMNFV 57065 (Fig. 9D). Resorption cavities in the deep cortex are limited across all studied fibulae, but fibula RGM.1394118 has numerous large immature secondary osteons.

3.7. Vertebrae

The *Triceratops* vertebrae show a high degree of secondary bone remodelling and the presence of growth lines (Fig. 10). The most proximal area of the neural spine of the dorsal vertebra RGM.1394100 still shows some amount of primary bone (Fig. 10A). The bone tissue is relatively well organized and contains numerous closely spaced growth lines that are overprinted by extensive remodelling. The vascularity consists of longitudinal primary osteons, but they occur in relatively low abundance throughout the primary bone. The amount of primary bone in the neural spine diminished greatly more distally as secondary osteons become more dominant and the medullary cavity covers relatively more area (Fig. 10A). The transverse processes of dorsal vertebrae show even stronger degrees of bone remodelling and contain a high number of large overlapping secondary osteons (Fig. 10B). The neural spine of the cervical vertebra produces a similar sequence in histological patterns but shows more extensive remodelling than the dorsal vertebra (Fig. 10C). The transverse process, on the other hand, preserves relatively more primary bone than seen for dorsal

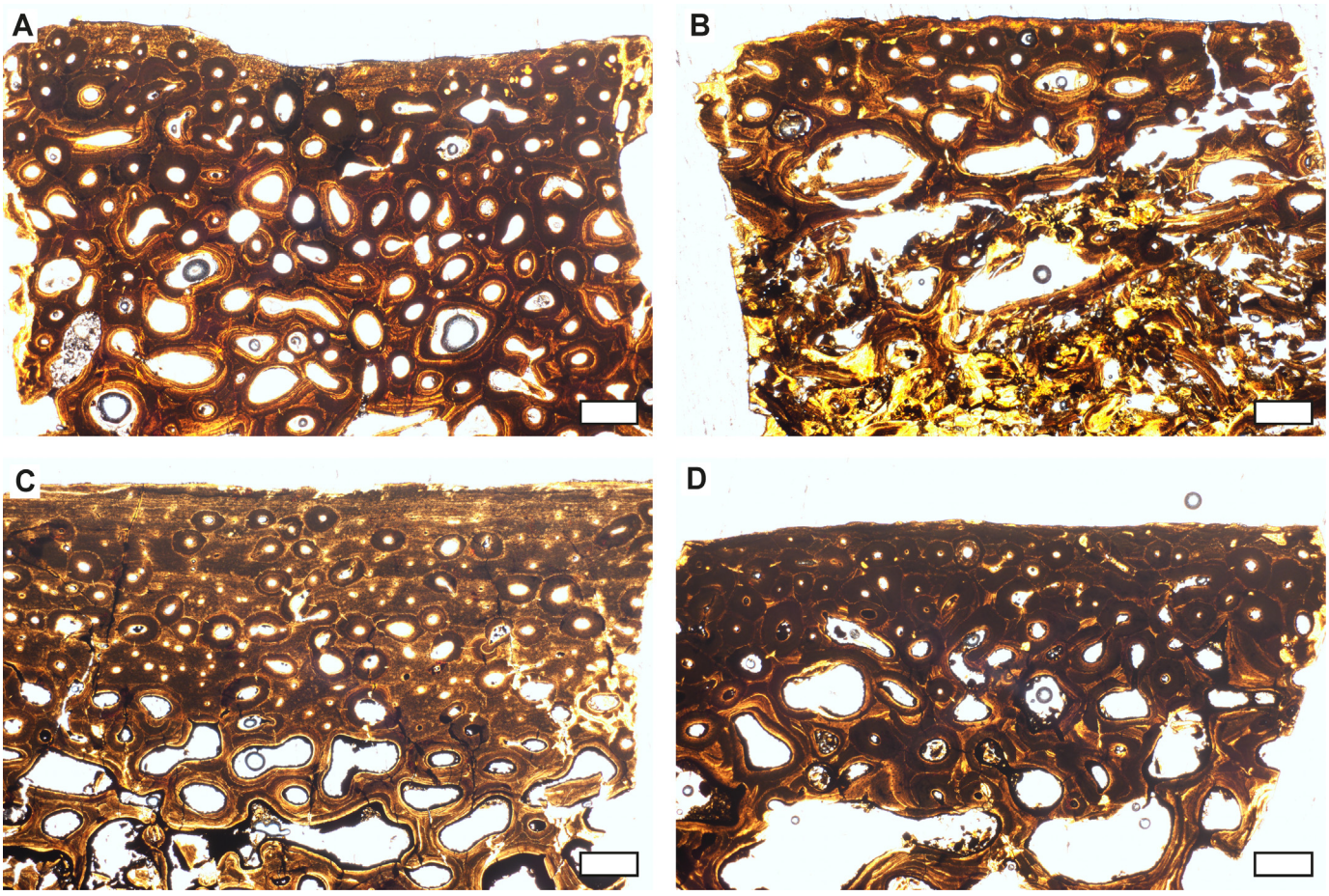

Fig. 10. Overview of *Triceratops* vertebrae histology. All images are in plane-polarized light as this provides the most ideal visualisation of histological markers due to section thickness. Bone surfaces are towards the top for all images. A. Histology of the neural spine of dorsal vertebra RGM.1394100. Bone remodelling is advanced, but the primary bone is relatively avascular and contains inconspicuous growth marks. B. Transverse process of the same element, with higher rates of bone remodelling. C. Histology of the neural spine of cervical vertebrate RGM.1394101. Remodelling is less pronounced than in dorsal vertebrae, but the primary bone also contains inconspicuous growth marks. D. Highly remodelled transverse process of the same element. All scale bars are 500 μm.

vertebrae (Fig. 10D). The small areas of preserved primary bone of cervical vertebrae are well-organised with only very few primary osteons. Bone remodelling is very extensive and large areas are remodelled into dense Haversian tissue.

3.8. Ribs

Rib sections from *Triceratops* are characterized by extensive bone remodelling (Fig. 11). Where primary bone is still preserved, there is predominantly woven bone in a woven-parallel complex made up of dense longitudinal primary osteons. These osteons are generally more abundant larger in diameter than those in limb elements. The primary bone of rib RGM.1394098 shows well-defined growth lines (Fig. 11A, C), but their occurrence does not follow a regular pattern. The most proximal and most distal sample (Fig. 1, sample #1 and #3) preserve clear growth lines, while the middle sample shows dense Haversian tissue (Fig. 1). However, the relative amount of preserved primary bone diminishes towards the distal end, probably because the HSF is relatively more advanced than in the more proximal parts (Fig. 11B). We do note that our sampling strategy for RGM.1394098 did not cover the complete length of the rib. Rib RGM.1394097 did not show any significant variation in histological markers across the sampling transect. All five samples (Fig. 1) showed very high degrees of remodelling with one or two inconspicuous growth marks. The relative abundance of secondary osteons was higher in more distal samples. Overall, the anterior regions of both ribs tend to show a lesser developed HSF and preserve more primary bone, including growth lines. The complete cross-section taken proximally reveals the same histological patterns (Fig. 12). The thicker lateral margins (Fig. 12A,B,C) show high numbers of secondary osteons and woven-parallel primary tissue with one or two growth lines consisting of more parallel-fibred bone tissue. More proximally, the capitulum shows a completely remodelled bone cortex of multiple generations of secondary osteons (Fig. 11D). All ribs show dense Sharpey's fibres in the preserved primary bone, reflecting the insertion of the intercostal musculature.

3.9. Skeletochronology

Triceratops deposits mostly layers (annuli) of parallel-fibred tissue instead of well-defined LAGs. However, out of all the 25 sampled limb bones (16 when only including humeri, femora and tibiae), only four preserve considerable numbers of cyclical growth marks in their primary growth record (Fig. 13). These include humeri RGM.1394102 and RGM.1394103, femur RGM.139414111 and tibia RGM.1394114. Thus, the majority of the larger limb elements (including humeri, femora, tibiae) as well as all smaller limb bones (including radii, ulnae, fibulae) do not preserve a cyclical growth record. The tibia sample preserves the highest number of growth cycles (16 combined zones and annuli), while the two humeri

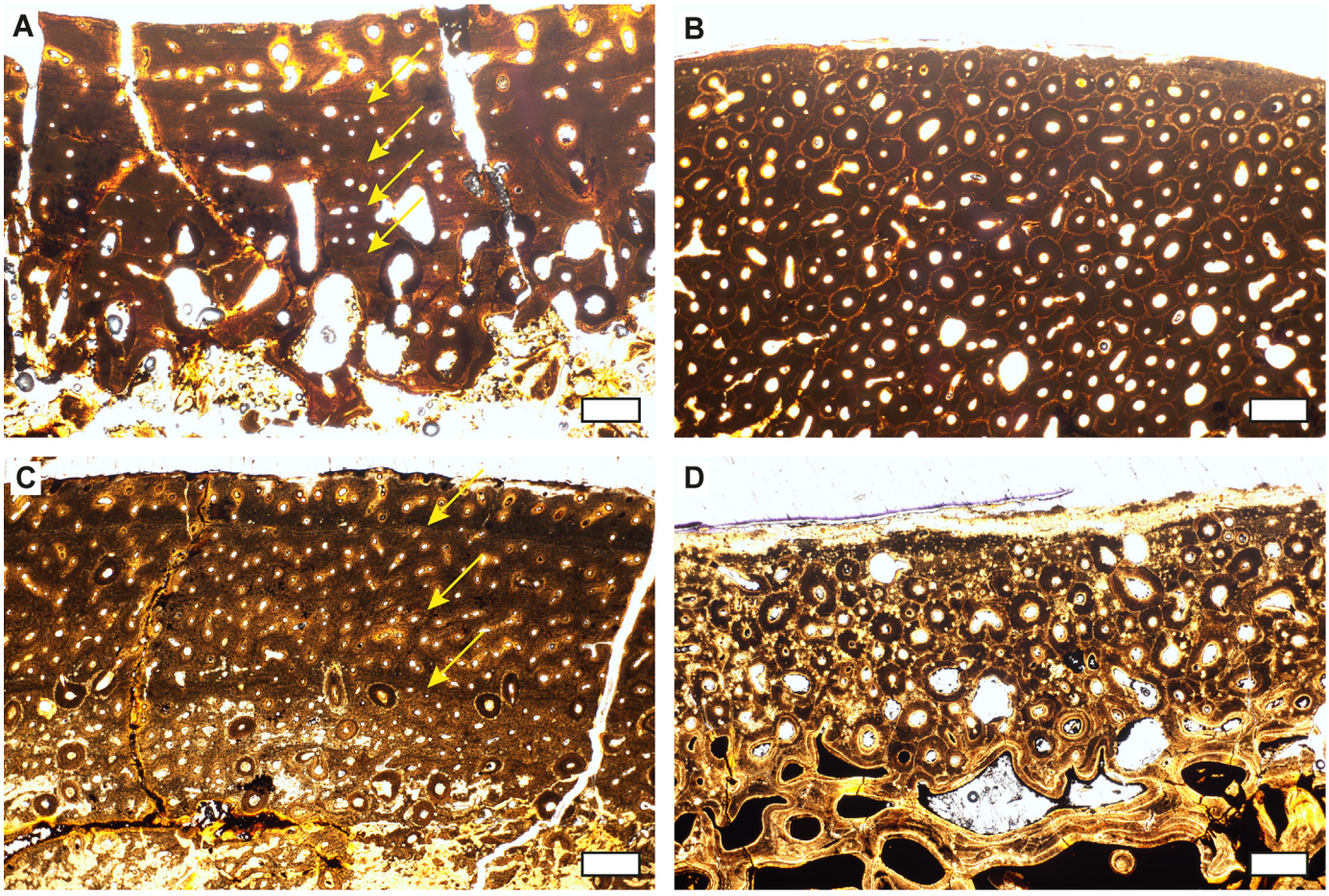

Fig. 11. Overview of *Triceratops* rib histology. All images are in plane-polarized light as this provides the most ideal visualisation of histological markers due to section thickness. Bone surfaces of the anterior side are towards the top for all images. A. Histology of most proximal area of the main shaft of rib RGM.1394098 showing strong vascularity as well as bone remodelling and resorption in the lower half of the section. The arrows indicate possible growth lines. B. More distal area of rib RGM.1394098 showing dense Haversian bone. C. Most distal sample of rib RGM.1394098 showing only minor degrees of secondary remodelling. The arrows indicate three well-defined growth lines. Vascularity is relatively high. D. Capitulum of rib RGM.1394097 showing extremely dense Haversian bone turning into cancellous bone inwards. All scale bars are 500 μm.

preserve very few growth marks (3 and 4 combined zones and annuli). The femur sample shows a total of 9 growth cycles. However, the preserved annuli of parallel-fibred bone are still poorly delineated from the surrounding faster-growing bone tissue. Moreover, the spacing of the recorded growth marks is irregular and does not follow the expected pattern of decreasing growth rates with ontogeny. Thus, the DTB *Triceratops* does not permit a detailed skeletochronological analysis given the limited preservation of a primary cyclical growth record in only a small number of elements as well as the inconsistent spacing of growth marks (see section 4.3).

3.10. Application of the three-front model to limb bones

Fig. 14 shows the three-front model applied to the histologically youngest and oldest *Triceratops* limb bones from the DTB. Note that these results are relative to each other and therefore can only be compared within the discussed framework of *Triceratops* histology. Nevertheless, these models provide a comprehensive overview of the observed histological patterns. The inter-elemental differences are most clearly expressed in the speed of the apposition front (AF) and resorption front (RF), because the relative cortical thickness seems the most defining characteristic for the observed histological patterns. The tibiae possess the thickest cortex, suggesting that the speed of the RF is relatively low compared to other limb bones. This explains the better preservation of primary bone in the deeper cortex of the tibiae, especially under the assumption of a constant speed of the Haversian substitution front (HSF, Mitchell and Sander, 2014) combined with a diffuse remodelling pattern seen in all limb bones. On the other hand, the humeri possess the thinnest cortex of all limb bone types, explaining our observation that the humeri show more advanced bone remodelling. In other words, constant remodelling rates across a thinner (i.e., resorbed) cortex will always result in relatively higher portions of secondary bone. Femora show the highest measured circumferences but have intermediate cortical thickness compared to the humeri and tibiae. The smaller limb elements such as the radii, ulnae and fibulae

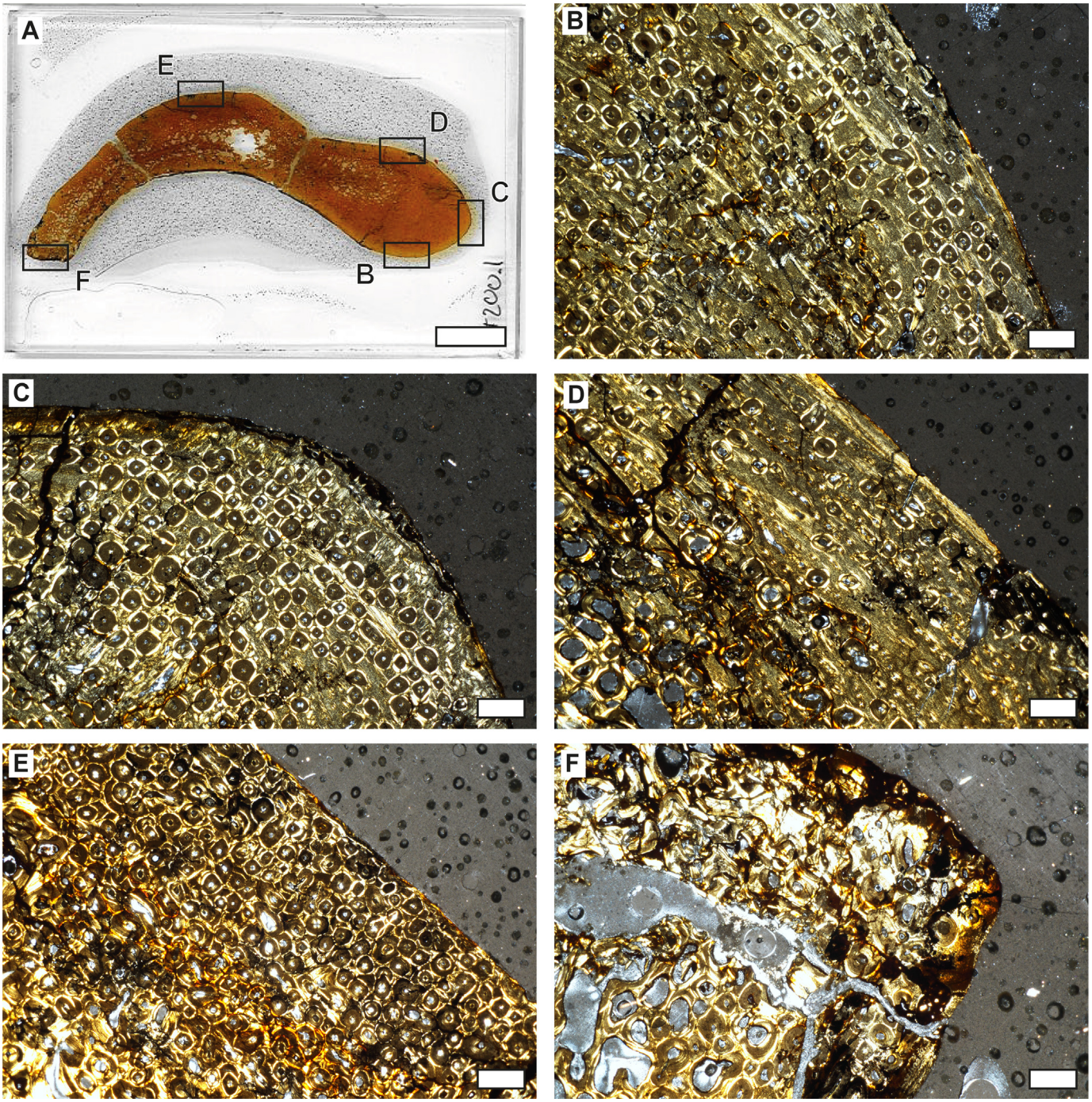

Fig. 12. Histology of RGM.1394121, the complete rib section. Generally, most of the cortical bone is heavily remodelled. A. Overview of the section with insets for each image. B. Histology of the posterolateral side showing many secondary osteons and longitudinal woven-parallel bone. There are two growth marks of parallel-fibred bone in the primary cortex being overprinted by secondary osteons. C. Most lateral section showing one zone of parallel-fibred bone and heavy bone remodelling. D. Histology of the anterolateral side showing relatively less bone remodelling. The primary woven tissue does not preserve any growth marks. E. Anterior portion showing dense Haversian tissue with multiple generations of secondary osteons. F. The most medial portion showing medullary expansion and bone remodelling. Scale bar for A is 1 cm and scale bar for B to F is 500 μm.

show the fastest AF as indicated by the mostly woven bone at the periosteal surface. The greatest differences in the three-front models of the older limb bones are mostly expressed in the AF. Especially the larger limb bones such as the humeri, tibiae and femora show significant decreases in bone apposition rates. This agrees with the observed larger zones of parallel-fibred bone that occur at the periosteal surface of larger (and presumably older) limb bones. Moreover, some bones (e.g., femur RGM.1394110) also deposit inconspicuous LAGs (Figs. 6 and 7), suggesting an even slower AF (Fig. 14). Curiously, the ulnae, radii and fibulae that were interpreted as being older do not show this decrease in AF speed and retain the same primary bone tissue at the periosteal surface

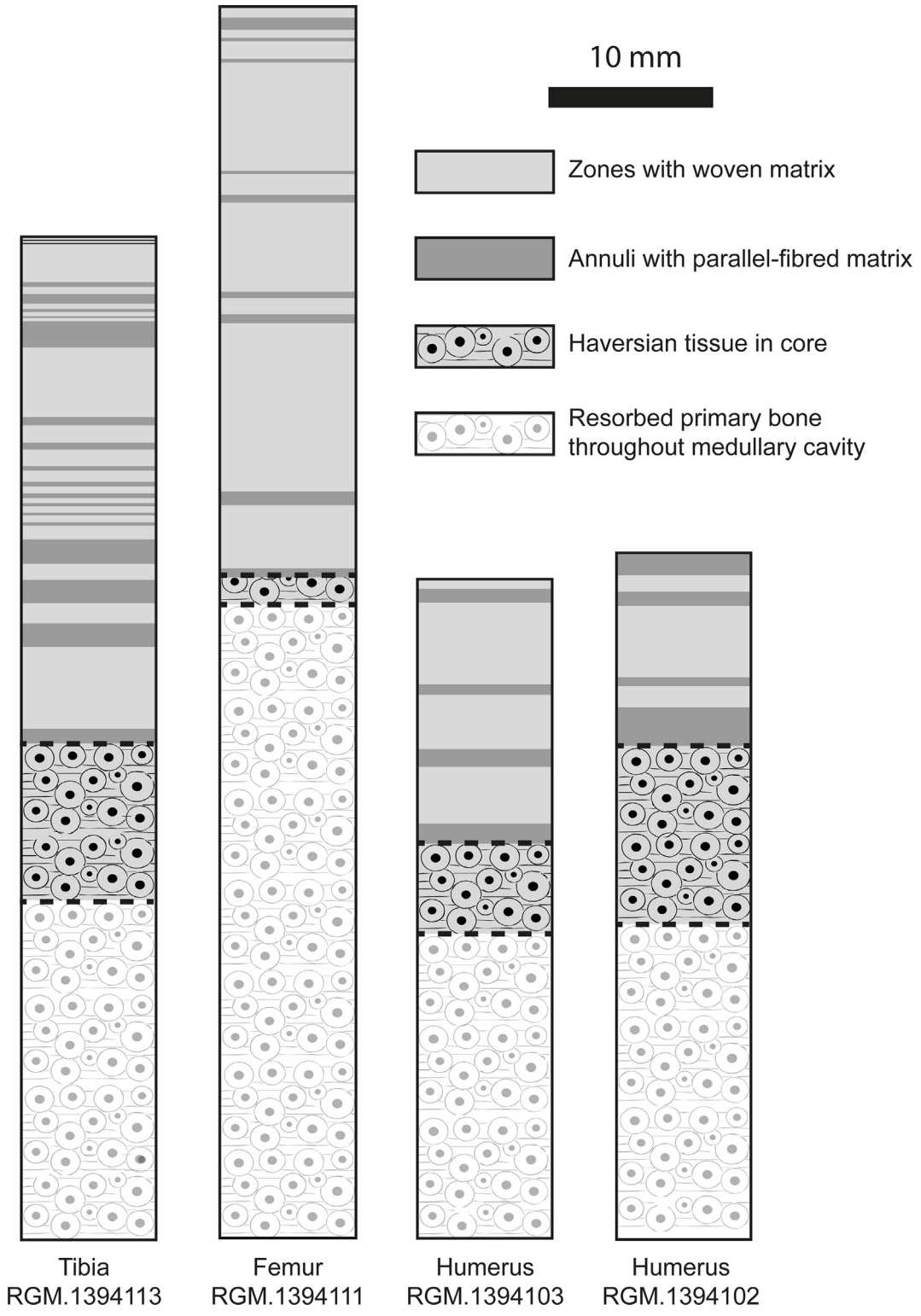

Fig. 13. Schematic representation of the skeletochronological markers in the core samples of the elements that preserved the most complete growth records. Tibia RGM.1394113 shows the highest number of preserved growth cycles. Note that a large portion of the growth record is obliterated by the HSF and RF, and that growth cycle spacing is irregular. The medullary centre is to the bottom and the bone surface is to the top for each of the four core drawings. Black dashed lines represent the boundary between zones indicated in the legend.

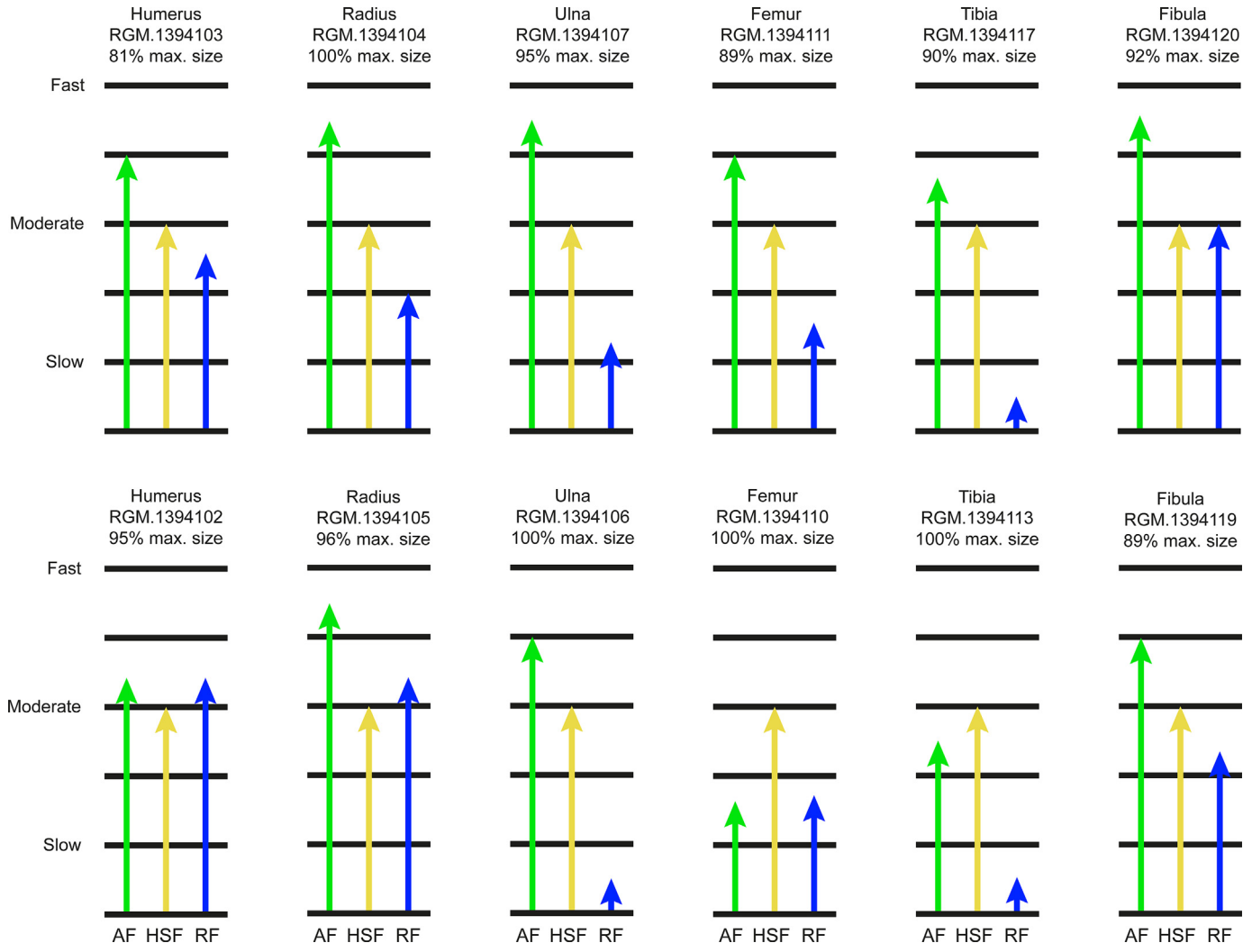

Fig. 14. Three-front models of the histologically youngest and oldest limb bones of the DTB *Triceratops*. The upper row represents the youngest elements of each limb bone type, and the lower row represents the oldest elements. The arrows indicate the (relative) speed of each of the fronts. The larger elements such as the femora and tibiae show the strongest shifts in the three fronts with ontogeny, especially in the apposition front, which is also indicated by the larger variety of primary bone tissue types seen in the histology. Smaller elements only show minor changes in the three fronts, and the radii and fibulae even show older histology in smaller elements. AF, apposition front; HSF, Haversian substitution front; RF, resorption front.

as their ontogenetically younger counterparts (Fig. 14). This suggests some allometry between the different limb bones in *Triceratops*.

3.11. Histologic ontogenetic stages

The difficulties in quantifying the primary growth record in *Triceratops* limb bones via skeletochronology call for the use of 'histologic ontogenetic stages' (HOS) to better capture ontogenetic changes in *Triceratops* histology (Klein and Sander, 2008; Mitchell et al., 2017; Sander and Wintrich, 2021). *Triceratops* shows a wide range of different bone tissue types within any given section, but the majority of the observed primary tissue types are defined by a combination of circumferential and longitudinal primary osteons as well as a combination of woven and parallel-fibred bone matrix. Accordingly, we were able to differentiate between five major bone tissue types (Fig. 15): circumferential woven-parallel bone (Type A), longitudinal woven-parallel bone (Type B), circumferential PFLC (Type C), longitudinal PFLC (Type D) and Haversian tissue (Type E). However, unlike in previous HOS studies (Klein and Sander, 2008; Sander and Wintrich, 2021), these tissues are not strictly laid down in an ontogenetic sequence except for Type E but are interspersed and repeat themselves. In other words, the proportions of multiple tissue types in a given element serve in defining the HOS. As both parallel-fibred and woven bone are observed in all elements and were already present in the smallest humerus RSM P.2691 (Fig. 2A), we assume that this histology is typical for *Triceratops* and that ontogenetic series will show these bone tissues. We do note that our current histological dataset does not cover the full ontogenetic range known for this taxon from skeletal material, and the DTB *Triceratops* mostly encompass relatively old individuals such as subadults and adults. However, we had extended the size and presumably age range by adding the smaller humeri RSM P.2691 and RSM P.3324.6.1 from Canada to our histological sample. Nevertheless, the lowest stage (HOS 1) in our scheme remains hypothetical.

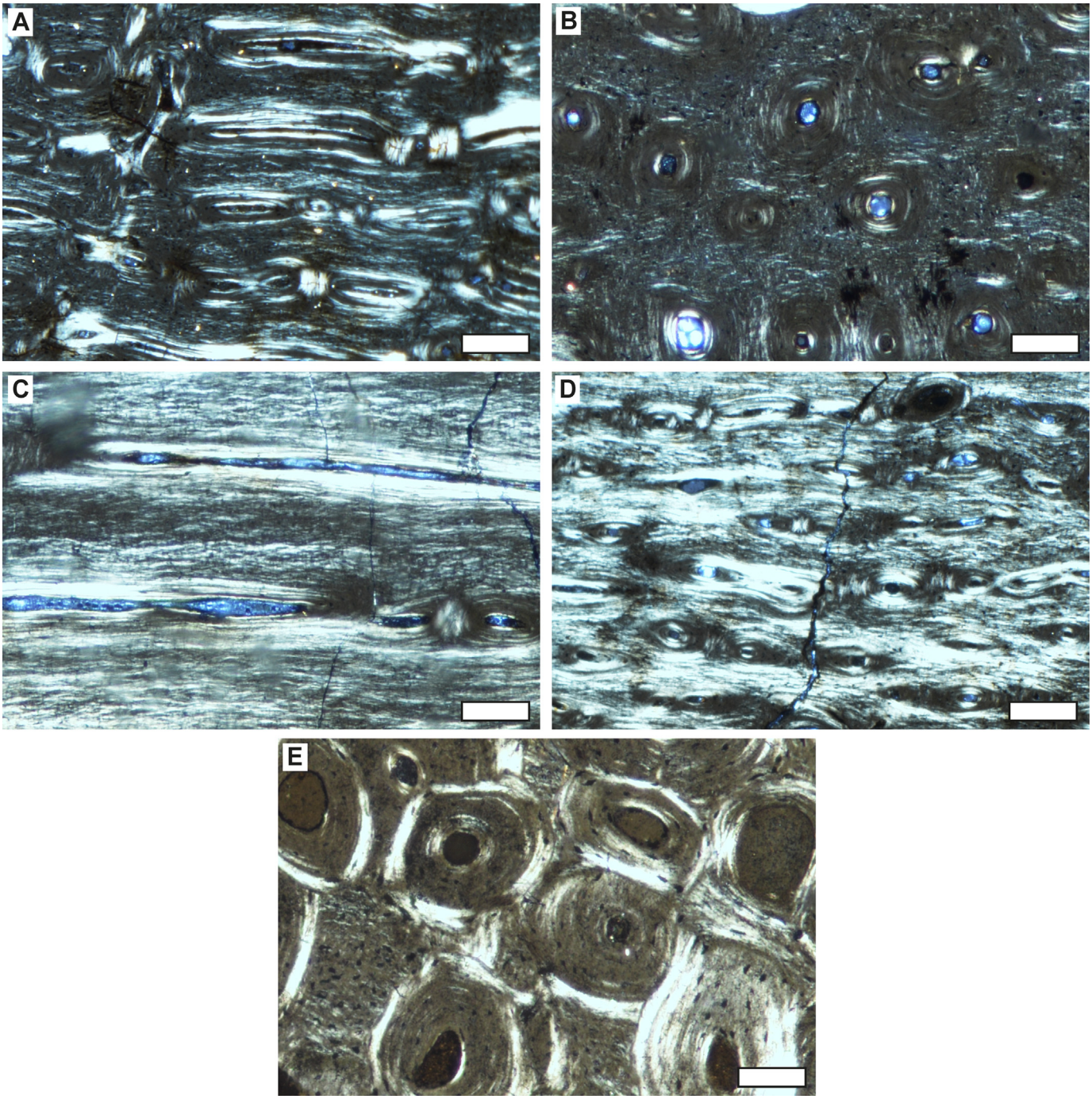

Fig. 15. Representative photographs of each of the five tissue types used in the HOS definitions for *Triceratops*. All photographs are in cross-polarized light. A. Tissue type A consists of laminar woven-parallel bone tissue. B. Tissue type B consists of longitudinal woven-parallel bone tissue. C. Tissue type C consists of laminar parallel-fibred bone tissue (i.e., laminar PFLC). D. Tissue type D defined as longitudinal parallel-fibred bone tissue (i.e., longitudinal PFLC). E. Tissue type E consists of Haversian bone tissue, albeit with some primary bone remaining. Scale bar for A and D is 200 μm, and scale bar for B, C and E is 100 μm.

Using the five tissue types, we described seven HOS corresponding to different biological ontogenetic stages (BOS) (Table 2). Each HOS is defined as a combination and sequence of each of the five tissue types (Table 2), and representative diagrams are found in Fig. 16. While these stages describe the most dominant histological patterns, some bones preserve a unique combination of tissue types that fall outside the HOS scheme. For example, fibula RGM.1394119 is placed in HOS 7 based on the presence of dense Type E bone tissue, but still shows simple vascular canals with woven bone at the periosteal surface typical of lower HOS. As these tissue types do not represent true HOS 7, they could be considered as transitional stages (i.e., HOS 6.5). In addition, we sporadically observed areas of radial and reticular woven-parallel bone tissue substituting for either circumferential or longitudinal woven-parallel bone. However, the current histological dataset is too limited to allow for a more detailed HOS scheme.

HOS and body size are highly correlated. Fig. 17 shows relative percentage maximum size (proxy for body size) plotted against their corresponding HOS for the humeri, femora and tibiae. The data shows the expected trend, where larger bones show higher

Table 2
Description of the histologic ontogenetic stages (HOS) for *Triceratops*. A total of seven stages were developed based on the occurrence of dominant tissue types (Fig. 16). HOS 1 was not available in the sample analysis but was extrapolated on the assumption that new-born animals have porous bone in general. HOS 3 was most likely available in humerus RSM P.3324.6.1, but the preservation is too poor to tell. Thus the description for HOS 3 was partially based on extrapolation from HOS 2 to 4. For each HOS we assigned a biological ontogenetic stage (BOS). The HOS assigned to the studied material can be found in Table 1.

HOS	Tissue types	BOS
1	The bone tissue consists of woven bone with a high number of laminar simple vascular canals.	Hatchling
2	Cortex consists of Type A with small zones/patches of Type B. The primary osteons are relatively large and have a thin lining of lamellar bone. They often resemble simple vascular canals. No bone remodelling. Vascularity is relatively high and consistent.	Early juvenile
3	Mostly Type A with conspicuous layers of Type B. Inconspicuous zones of Type C that are mostly restricted to the periosteal surface. Lamellar bone of the primary osteons are well-defined, and primary osteons have become relatively small.	Late Juvenile
4	Type A with clear patches of Type B in the outer half of the cortex. Type C becomes more apparent as annuli throughout the primary bone, as well as occurring randomly within the zones of Type A and B. Bone remodelling in the form of secondary osteons is restricted to deeper parts of the cortex. Vascularity is high, but is generally lower close to the areas of Type C.	Early subadult
5	The majority of the cortex shows thin zones of Type A and B, separated by thicker conspicuous areas of Type C. Bone remodelling is over halfway of the cortical bone, and the tissue close to the periosteal surface now shows immature secondary osteons. Type E is restricted to the very deep cortex. Vascularity remains constantly high, but slightly decreases in zones of Type C close to the bone surface. Type A and B may also sporadically show reticular or radial primary canals. Simple vascular canals may still be present and are restricted to the outermost periosteal surface, sometimes opening at the bone surface.	Late subadult
6	The preserved primary tissue shows higher numbers of layers of Type C and D of various thickness, and the primary cortex becomes more organized. Type A and Type B only occur as poorly vascularized layers, mostly near the periosteal surface, but even here the tissue is relatively more organized as parallel-fibred tissue is mixed in. When unorganized bone is present, Type B is than more dominant. There are no simple vascular canals. High numbers of secondary osteons appear close to the bone surface, but overall show a diffuse pattern. Type E progresses closer to the bone surface and covers more than half of the cortical thickness. Inconspicuous LAGs may form just beneath the periosteal surface indicating skeletal maturity.	Adult
7	Type E overtakes large portions of the cortical bone, and LAGs become more numerous, and may form an EFS. Primary tissue is limited to close to the periosteal surface, but may still show any tissue type depending on the element.	Mature

HOS, and thus are considered ontogenetically older. However, it should be noted that elements that have the same HOS stage may still differ in number of secondary osteons, growth lines, simple vascular canals, as well as local vascular organisation. Thus, while a general ontogenetic pattern exists, the proposed tissue types and HOS stages should not be considered definitive, and their interpretation warrants some degree of flexibility. A refined HOS scheme with more HOS will require a substantial increase in sample size and body size range.

4. Discussion

4.1. Dominant primary histology and growth patterns

Like many non-avian dinosaurs and other fast-growing vertebrates (Margerie et al., 2004; Margerie et al., 2002), *Triceratops* shows typical woven-parallel bone tissue with a mixture of longitudinal and circumferential primary osteons. However, the bone matrix organization within the observed bone tissue type is not strictly fibrous/woven. Instead, the matrix surrounding the vascular network of primary osteons in cortical bone is often characterized by parallel-fibred bone tissue (e.g., Fig. 8). Especially the larger limb elements such as humeri, tibiae and femora show this specific histological feature increasingly more towards the bone surface (e.g., Fig. 5D). As a result, *Triceratops* long bones possess a distinct type of parallel-fibred 'fibrolamellar' bone tissue. A similar type of tissue has previously been described in limb bones of certain sauropod dinosaurs including *Ampelosaurus* and *Magyarosaurus*, in which the initially deposited scaffold of the primary bone is parallel-fibred instead of woven (Stein et al., 2010; Klein et al., 2012). Klein et al. (2012) proposed the term 'modified laminar bone' (MLB) to describe this unique histology of relatively slower bone apposition rates. However, the studied *Triceratops* primary bone is not characterized by a predominantly laminar organisation, but instead shows dense longitudinal vascularity. Therefore, we propose the more generalized term 'parallel-fibred lamellar complex' (PFLC) to discuss the dominant primary histological patterns observed here for *Triceratops*. The longitudinal primary osteons are almost always positioned in circumferentially oriented rows parallel to the bone surface, creating bone laminae similarly to those seen in true laminar woven-parallel bone (e.g., compare Fig. 7A and 7B). So while the term 'modified laminar bone' might not accurately describe the tissue in *Triceratops*, there is a strong resemblance of PFLC with MLB. In addition to the longitudinal canals, the humeri and femora sporadically show zones of radial woven-parallel bone (Figs. 2E and 5A, D).

Many large-bodied non-avian dinosaurs such as sauropods, theropods, and ornithopods predominantly show well-vascularized woven-parallel bone with limited growth marks throughout the primary cortex, indicating rapid uninterrupted growth (Buffrénil et al., 2021; Cullen et al., 2020; D'Emic et al., 2023; Horner et al., 2000; Sander et al., 2011). However, the ontogenetically increasing amount of parallel-fibred bone associated with flat osteocytes and lower vascularity suggests an overall slower growth rate for *Triceratops* (Margerie et al., 2004; Margerie et al., 2002). While this dataset only partially covers ontogenetically young *Triceratops* material, the presence of parallel-fibred 'fibrolamellar' bone in a medium-sized humerus (RSM P.3324.6.1 of 550 mm) suggests that the onset of these bone tissue changes already occurred at an early (ontogenetic) stage.

4.2. Patterns of bone remodelling explained by the three-front model

All of the studied limb elements except for the two smallest humeri show extensive bone remodelling. The ulnae and radii preserve only very little amounts of primary bone close to the bone surface. This primary tissue mainly consists of longitudinal woven-parallel bone but is quickly overprinted by the advancing HSF, i.e., secondary osteons that grade into Haversian bone towards the

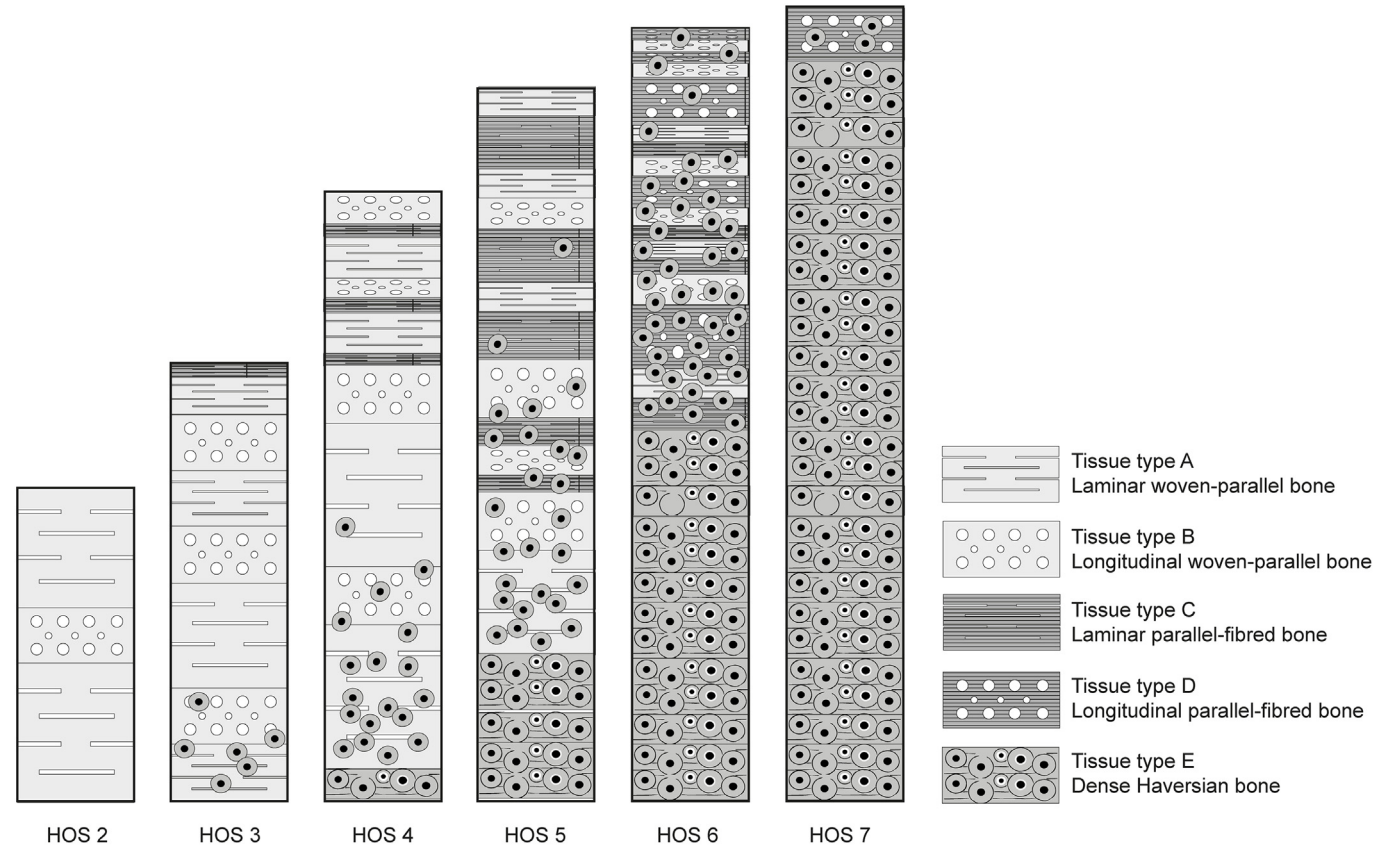

Fig. 16. Diagrams showing the combination of bone tissue types defining HOS 2 to 7. Note that HOS 1 is currently hypothetical. The increase in column length from left to right is to visualize ontogenetic increase in cortical thickness. The increase is not to scale.

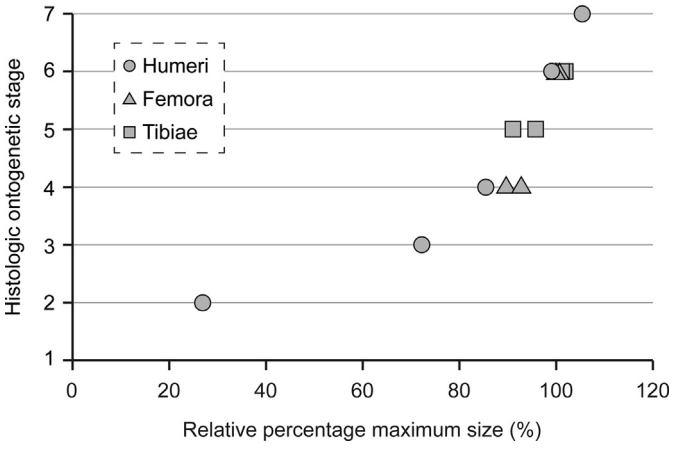

Fig. 17. Relationship between size and HOS for the humeri, femora and tibiae. Element size is relative percentage to calculated maximum size (Table S1). Each bone type shows a predictable pattern, where increased bone lengths correspond to higher HOS, and presumably older individuals. This pattern is best developed in the humeri because of the wide size range sampled. The close correlation between HOS and size is consistent with the sampled bones representing a single biological genus, i.e., *Triceratops*.

medullary cavity, which apparently advances with a constant rate in all bones regardless of their size (Mitchell and Sander, 2014). Thus, the overall high degree of bone remodelling reflects the small size of elements including the radii and ulnae, as thinner bone cortices are more rapidly overtaken by the HSF. The larger limb elements conform to this same pattern of the size-independent advance of the HSF, and preserve more primary bone due to having thicker cortices. Fibulae preserve little primary bone but also lack dense Haversian tissue. Almost all humeri show larger areas of primary bone, except the largest – and presumably oldest – humerus P.1163.9, where remodelling has advanced to the bone surface (Fig. 2F). The tibiae and femora also show lower amounts of secondary remodelling and have relatively high portions of preserved primary bone tissue. For all limb elements, extremely dense Haversian tissue is very limited, and large parts of cortical bone preserve interstitial primary tissue. In other words, *Triceratops* and presumably other ceratopsians differ from some other dinosaurs in that the HSF is diffuse and overlapping secondary osteons are often limited to two generations, even in the deepest cortical bone of complete core-samples. Taxon-specific differences in the HSF were already noted for sauropods by Sander (2000).

The observed inter-elemental differences in bone remodelling patterns can also be conceptualized by the three-front model. Humeri and tibiae that have overlapping bone dimensions (e.g., bone length and circumference at sampling location, Table 1) show an equally advanced HSF close to the periosteal surface. For example, the larger elements such as humerus RGM.1394102 (length 761 mm and circumference 382 mm) and tibia RGM.1394114 (length 781 mm and circumference 355 mm) from the DTB both show an HSF advanced close to the periosteal surface. These observations fall in line with the constant rate of bone remodelling, and thus constant speed of the HSF assumed by Mitchell and Sander (2014). However, tibiae (and femora) in general still preserve significantly thicker cortical bone than humeri (Table 1, Fig. S1). This is also reflected in the three-front models, showing that the RF in humeri is significantly faster than in tibiae and femora (Figs. 14 and 15). As a result,

the humeri will always have higher portions of secondary bone and a larger medullary cavity compared to the tibiae and femora, despite a constant rate of the HSF. This pattern is even observed within the same individual. Thus, the observed bone remodelling patterns and distribution of histological markers are best explained by the analysis of the three-front model.

The proportionally large *Triceratops* cranium represents a relatively high volumetric percentage of the entire skeleton, especially in later ontogenetic stages, and must have exerted great biomechanical loading. Estimates of the centre of body mass and axial mass distributions in the chasmosaurine *Chasmosaurus* hinted at an anteriorly inclined loading direction (Henderson, 2014). A similar loading regime in *Triceratops* should translate to relatively higher rates of remodelling in the forelimbs compared to the hindlimbs. This hypothesized pattern is observed in the *Triceratops* histological dataset presented here. The forelimbs show an overall more advanced remodelling front as evidenced by the multiple generations of secondary osteons as well as near-complete overprinting of the primary cortex in the radii and ulnae. We do note that possible size differences between different types of elements could also contribute to the observed remodelling patterns in fore- and hindlimbs as mentioned above. However, the lesser degree of remodelling in the cortex of the fibulae compared to the pronounced remodelling in radii with equally thick cortices (Table 1) suggests that additional factors such as biomechanical loading may play a role in *Triceratops* bone remodelling.

4.3. The absence of a primary growth record in appendicular and axial bones

Despite the extensive histological analysis performed on a large selection of *Triceratops* postcranial material, we were able to retrieve only very limited skeletochronological data. Growth cycles were exclusively expressed as layers of parallel-fibred bone tissue and did not follow a predictable growth pattern with ontogeny (Fig. 13). The elements that preserved the most complete primary growth record (e.g., tibia RGM.1394114) provided insufficient data for the calculation of realistic ages-at-death and annual bone apposition rates. The lack of a visible growth record in *Triceratops* is most likely not related to overprinting by secondary osteons. On the contrary, the bone remodelling patterns are relatively diffuse in many of the studied limb bones, and primary cortical bone often remains visible even in deeper areas of the cortex. Thus, it seems that *Triceratops* does not preserve a primary growth record in the first place, or at least complete enough for skeletochronological analyses. These same findings were obtained for large-bodied sauropods (Sander, 2000; Klein and Sander, 2008; Sander et al., 2011) where it is argued that cyclical growth marks were not deposited due to the high growth rates of the especially large limb bones. However, *Triceratops* shows relatively slower bone apposition rates as indicated by the large portions of parallel-fibred bone, but still does not preserve a clear primary growth record. More ontogenetically extensive datasets on *Triceratops* bone histology as well as other derived ceratopsians may reveal whether a lack of primary growth records is characteristic for the whole group.

In sauropods, the ribs show a significantly more complete primary growth record and make up for the poor record in limb bones (Waskow and Sander, 2014; Waskow, 2019). It is argued that the absolute smaller sizes of ribs elicit lower growth rates and more periodical growth cessations. Considering the histological similarities between sauropods and *Triceratops*, it is expected that *Triceratops* may reveal similar discrepancies between limb and rib histology. However, the axial elements of *Triceratops* studied here show ambiguous results regarding the preservation of a primary growth record. The ribs that were sectioned proximal to distal reveal inconsistent patterns, where distal samples show a more advanced HSF compared to proximal samples, despite the fact that distal rib regions represent younger bone tissue. The complete rib section from RGM.1394121 preserves a high number of secondary osteons that overprint the majority of the primary tissue. The primary cortex is limited to the periosteal surface and contains only a small number of inconspicuous growth lines. This observation is contrasting to the sauropod rib sections that show little remodelling and a high number of growth lines in the primary tissue (Waskow and Sander, 2014). Samples of the vertebrae show equally ambiguous trends in sequential histological patterns along the proximal–distal transect. The primary tissue contains inconspicuous growth marks, but the Haversian bone overprints the majority of these markers, and does not enable accurate growth record reconstructions.

Thus, the remodelling front is more extensive in *Triceratops* ribs than in previously recorded non-avian dinosaurs (Waskow and Sander, 2014; Waskow and Mateus, 2017). Hedrick et al. (2020) reported similarly strong remodelling patterns in the ribs of the centrosaurine dinosaur *Pachyrhinosaurus perotorum*. The authors argued that changes in rib shape as well as strong environmental influences resulted in increased remodelling rates of *Pachyrhinosaurus* ribs. The same lines of reasoning can be applied to the *Triceratops* ribs and vertebrae studied here, but it does not explain the differences seen between sauropods and ceratopsians. Overall, the current data on ceratopsian histology shows that ribs have equally inconsistent preservation of the primary growth record as limb elements, suggesting that the axial elements are poor candidates to study the growth and development of this group of dinosaurs. However, additional research on ceratopsian histology is needed to confirm if this pattern of rib growth also extends to a larger majority of the group.

4.4. Ontogenetic signal in *Triceratops* limb bone histology

Both the three-front models and the HOS follow an expected pattern consistent with an ontogenetic growth series of a single species. All limb bone samples lie on the same growth trajectory. For almost every element type (Fig. 14), the three-front models show a decrease in the AF consistent with lower growth rates expected for older individuals. Along the same lines, the elements that show a faster AF were also assigned a lower (i.e., younger) HOS. However, the two methods show minor offsets in histological identification. The three-front model indicates that there is a difference between the tibiae, femur and humerus – albeit small – specifically in the AF and RF. This would indicate that some elements may show a lower or higher growth rate. However, all four of the associated elements are assigned to the same HOS 6, suggesting that these elements have similar growth patterns.

The offset in growth pattern identification between both methods is most likely a result of the specific parameters used to describe the three-front models and HOS. In our three-front models, we only distinguished between bone matrix organisation to define the AF and did not consider the different types of vascularity observed in the sections (cf. Mitchell and Sander, 2014). In the HOS scheme, on the other hand, vascularity plays a major role in defining the histological position of the studied limb bones, but does not describe relative intra-bone variations seen in multiple fronts. For example, humerus RGM.1394102 shows a relatively poorly vascularized periosteal surface, but also possesses larger portions of woven-parallel bone tissue compared to the corresponding femur and tibia, giving it a relatively faster AF. However, the portions of woven-parallel bone show mostly longitudinal vascularisation, which would suggest a lower growth rate than

laminar woven-parallel bone tissue when compared in the HOS scheme. Moreover, RGM.1394102 shows high densities of secondary osteons which is not considered by the three-front model, but is a determining factor in the HOS scheme. Thus, while the three-front models mostly describe specific relative histological differences within a set of samples, the HOS provide an alternative way of visualizing more general ontogenetic changes. Taken altogether, the ontogenetic placement of the *Triceratops* elements is most accurate when the three-front models and HOS are combined, and their analysis allow to better constrain the changes in *Triceratops* growth and ontogeny. While there are some minor deviations in age-size distributions, the overall pattern shows an expected relation between size and histology (Fig. 17), indicating that individuals with larger body size represent ontogenetically older *Triceratops*.

4.5. Phylogenetic patterns of ceratopsian growth

The histology of non-ceratopsid ceratopsians has been studied more extensively than that of ceratopsids, and may provide insights on the evolution of ceratopsian growth patterns when combined with insights gained on *Triceratops* in this study (Fig. 18). *Psittacosaurus* represents one of the most basal members of Ceratopsia, and a total of three *Psittacosaurus* species have been studied for their bone histology including (from most basal to most derived) *P. mongoliensis* (Erickson and Tumanova, 2000), *P. lujiatunensis* (Zhao et al., 2019) and *P. sibiricus* (Skutschas et al., 2021). While there are some marked differences in vascularisation and bone remodelling, many of the studied *Psittacosaurus* species show recurring histological patterns. All three *Psittacosaurus* species show predominantly reticular vascular organisation and much woven bone in earlier ontogenetic stages, while the *Triceratops* juvenile humeri consisted of a mix of longitudinal and circumferential vascular canals. However, *P. lujiatunensis* and *P. sibiricus* deposit parallel-fibred bone and longitudinal canals only at the oldest observed ontogenetic stage – markers that can already be seen in earlier stages in *Triceratops*. *P. mongoliensis* retains reticular woven-parallel bone tissue even in larger/older individuals. Bone remodelling is only evident in very late ontogeny in *P. lujiatunensis* and *P. sibiricus* but is not seen in *P. mongoliensis*, while *Triceratops* starts bone remodelling at an earlier ontogenetic stage. All *Psittacosaurus* species show LAGs starting from the juvenile stage suggesting that they expressed periodic growth stops already early in ontogeny. This contrasts with ceratopsids such as *Triceratops* that show continuous growth with LAGs only appearing very late in ontogeny. A similar trend is seen between more basal sauropodomorphs and derived sauropods (Sander et al., 2011; Botha et al., 2022).

Koreaceratops hwaseongensis – as a non-coronosaur neoceratopsian – is more derived than *Psittacosaurus* and shows markedly different bone histological patterns (Baag and Lee, 2022). The *Koreaceratops* tibiae show a mix of longitudinal and circumferential vascular canals throughout the entirety of the primary cortex. *Triceratops* shows the same two dominant vascular

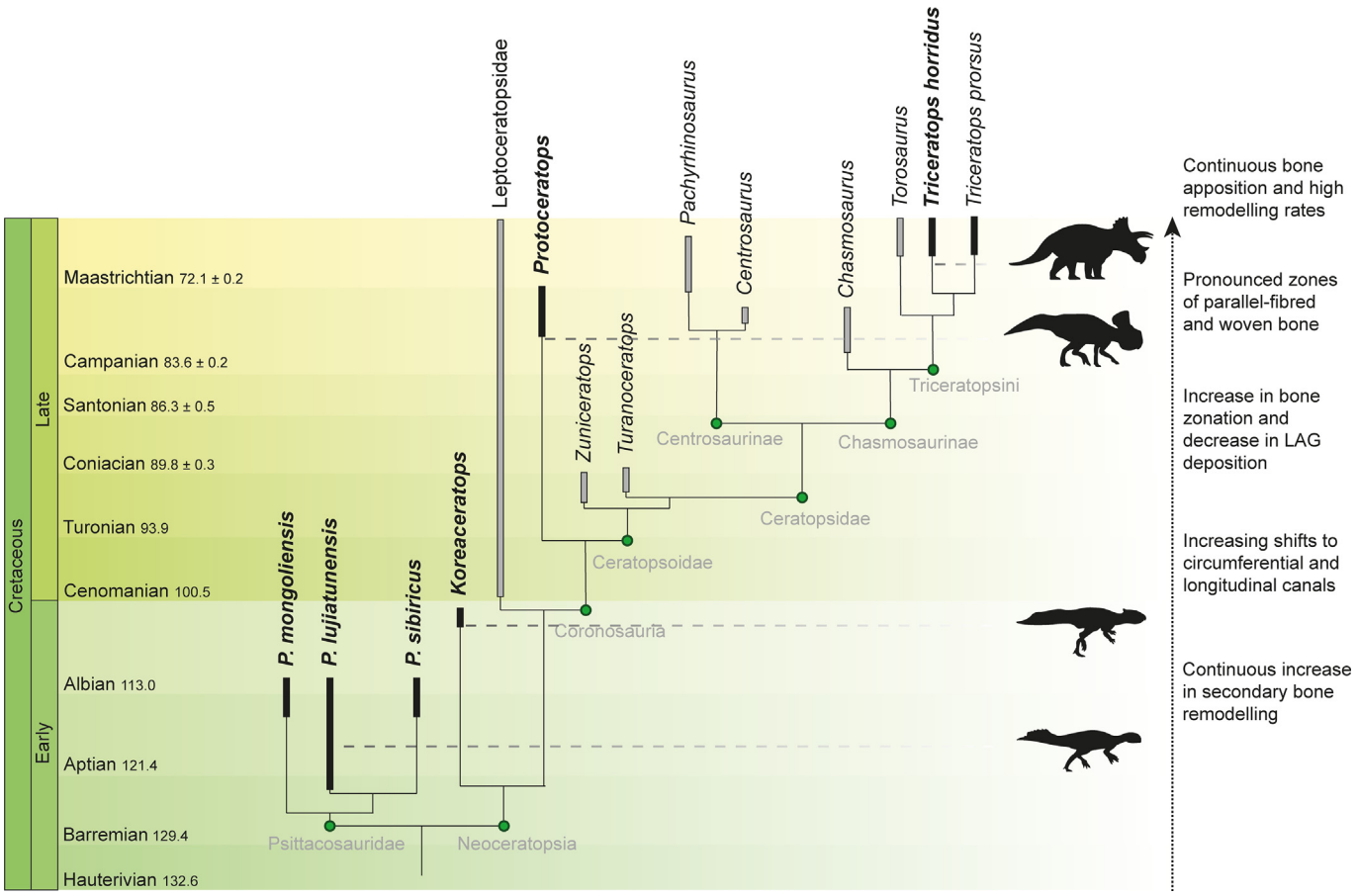

Fig. 18. Phylogenetic tree of all major groups within Ceratopsia. Highlighted in black and by silhouette are the taxa for which extensive histological data is available and compared here. Phylogenetic relationships and age ranges for each group are based on literature data (Wolfe et al., 2007; Sues and Averianov, 2009; Sampson and Loewen, 2010; Sereno, 2010; Lee et al., 2011; Zheng et al., 2015; Mallon et al., 2016), and are broadly used to indicate the relationship between the highlighted taxa. Time periods are based on stratigraphy.org. Silhouette are from phylopic.com. *Psittacosaurus* silhouette by Skye McDavid; *Koreaceratops* silhouette based on work from Park Jin-Young and Son Minyoung; *Protoceratops* silhouette by Andrew A. Farke; *Triceratops* silhouette by Raven Amos.

organisations in all of the studied limb elements, but may also show variable vascular patterns such as radial and reticular canals. The vascular density in *Koreaceratops* alternates between presumable zones and annuli (Baag and Lee, 2022). Unfortunately, the preservation of the studied *Koreaceratops* material did not allow for accurate estimates of bone tissue organisations, but the colour offsets and spacing of the different zones strongly suggest that the changes in vascular density coincide with shifts in bone tissue organisation (Baag and Lee, 2022). These cyclical patterns in woven and parallel-fibred bone tissue are also observed in *Triceratops* limb bones and are especially well-preserved in one tibia (Fig. 8). Moreover, the degree of bone remodelling in the *Koreaceratops* tibiae was significantly lower than in the fibulae.

The similarity in histology between basal ceratopsians and ceratopsids becomes clearer when comparing *Protoceratops* to the *Triceratops* data here. *Protoceratops* is a member of the Coronosauria, falling just outside the more derived group of ceratopsoids, and shows clearer alternating zones of parallel-fibred and woven bone (Fostowicz-Frelik and Słowiak, 2018). These cyclical patterns are patchy in juvenile specimens, but become pronounced in the sub-adult stage. This sequence is also observed in *Triceratops*, where parallel-fibred bone is deposited in early ontogeny and becomes more abundant in later stages. However, there is no clear cyclicity observed in the *Triceratops* primary growth record. Nevertheless, as in *Triceratops*, the cyclical zones are most numerous and best preserved in the tibiae of *Protoceratops* and rarely culminate in a growth line. It is not stated whether the parallel-fibred bone matrix of *Protoceratops* is deposited in conjunction with primary osteons (similar to the PFLC) or remains purely avascular, but the illustrations in the paper showing centripetally infilled primary osteons suggests the former (Fostowicz-Frelik and Słowiak, 2018).

The histological characteristics in *Triceratops* can be traced back to more basal non-ceratopsid ceratopsians. Curiously, *Triceratops* – as one of the most derived ceratopsian – seems to preserve a relatively basal aspects regarding their growth regime, as the appearance of parallel-fibred growth zones is already evident in *Koreaceratops* (~103 Ma) and becomes more pronounced in *Protoceratops* (~73 Ma) and ultimately dominant in *Triceratops* (~67 Ma). We do note that the current taxonomic coverage may be too limited to extrapolate these findings. However, the currently available data suggests that – throughout the evolution of ceratopsian dinosaurs – species developed a more continuous growth pattern as indicated by the increasing absence of growth lines and ambiguity of a primary growth record in more derived taxa.

4.6. Comparison with other ceratopsids

Little has been published in the peer-reviewed literature on the histology of ceratopsids which makes it difficult to accurately compare the *Triceratops* histology to other closely related taxa. It has been suggested that centrosaurines and chasmosaurines mainly differ in skeletochronological preservation and degree of bone remodelling, with the latter preserving overall fewer growth marks and higher remodelling rates (Reizner, 2010; Levitt, 2013; Hedrick et al., 2020). Within the centrosaurine data of Hedrick et al. (2020), the *Avaceratops* humerus preserved a single LAG in the mid-cortex of the humerus, while *Yehuecauhceratops* showed up to five LAGs near the periosteal surface of the femur, corroborating their estimated ontogenetic status. However, the *Triceratops* adult femur RGM.1394111 preserves up to seven LAGs near the periosteal surface. Moreover, the described bone remodelling for *Yehuecauhceratops* is equivalent to that of late sub-adult *Triceratops*, and the current published data suggest that centrosaurines and chasmosaurines have more overlapping bone histological patterns than previously thought.

However, these previously published assumptions on ceratopsid histology are based on the study of fragmentary material which have not allowed for in-depth comparisons of ceratopsian histology along the lines of phylogeny and ontogeny. On the other hand, unpublished work on the centrosaurine *Einiosaurus procurvicornis* has provided novel insights into its growth regime (Reizner, 2010), but the sample set only comprises juveniles and sub-adults not older than six years (based on LAG count). Therefore, it is difficult to predict whether the lack of bone remodelling in this species is an effect of taxonomic differences or simply because these specimens represent ontogenetically young individuals that yet need to remodel. Likewise, an unpublished thesis on the chasmosaurines *Utahceratops gettyi* and *Kosmoceratops richardsoni* provided some of the first datasets on chasmosaurine limb bone histology (Levitt, 2013), but the sampled material was mainly from presumed juvenile or sub-adult individuals. Considering the very late appearances of growth lines in *Triceratops*, the absence of LAGs in the young adult *Utahceratops* femur could have been an ontogenetic signal and not necessarily a marked difference between centrosaurines and chasmosaurines. Additional ontogenetically well-constrained ceratopsid limb material is needed to better understand the taxonomic implications of the observed histological offsets. Especially the first large-bodied ceratopsians, such as the ceratopsoids (e.g., *Zuniceratops* and *Turanoceratops*), may yield valuable insights into the evolution of ceratopsid growth strategies.

4.7. *Triceratops* species and *Torosaurus*

The *Triceratops* sections presented here can be compared between the two different species as well as with the available *Torosaurus* histology in the literature to provide additional context for potential species differences and for the taxonomic ambiguity between *Triceratops* and *Torosaurus*. Offsets between HOS and body size have previously been associated with potential taxonomic differences and/or sexual dimorphism (Klein and Sander, 2008; Redelstorff and Sander, 2009). For over a decade, there has been debate on whether *Torosaurus* is a valid genus or rather synonymous with *Triceratops* as its final ontogenetic stage (Scannella and Horner, 2011, 2010; Longrich and Field, 2012; Maiorino et al., 2013; Mallon et al., 2022). Previous hypotheses were mostly based on cranial characteristics including skull morphometrics, suture closing, transitional fossils and osteohistology of cranial elements. However, recently Mallon et al. (2022) provided the first images of *Torosaurus* limb bone histology. Their femur sections allowed to determine the relative age of a *Torosaurus* specimen more accurately. Based on the lack of an EFS, widely spaced secondary osteons at the bone surface and overall woven-fibred bone tissue, Mallon et al. (2022) concluded that their *Torosaurus* specimen did not reach skeletal maturity, and most likely represents a sub-adult individual. Fig. 19 shows the relationship between HOS and bone circumference normalized to femur circumference for the two *Triceratops* species as well as the *Torosaurus* femur section. The *Torosaurus* specimen can be assigned to HOS 5 transitioning into HOS 6 based on the published histological description, while our oldest *Triceratops* femur shows advanced HOS 6. However, the *Torosaurus* femur does not strongly deviate from the observed correlation between age and size for *Triceratops*, implying that both taxa are indistinguishable based on histology alone (Fig. 19).

Similarly, our results do not find a clear difference in HOS and body size correlation between *T. horridus* and *T. prorsus*. We do observe that the *T. prorsus* specimens are larger than the *T. horridus* specimens, but they also show the highest HOS in the dataset (Table 1, Fig. 19). Thus, it is still reasonable to assume that the

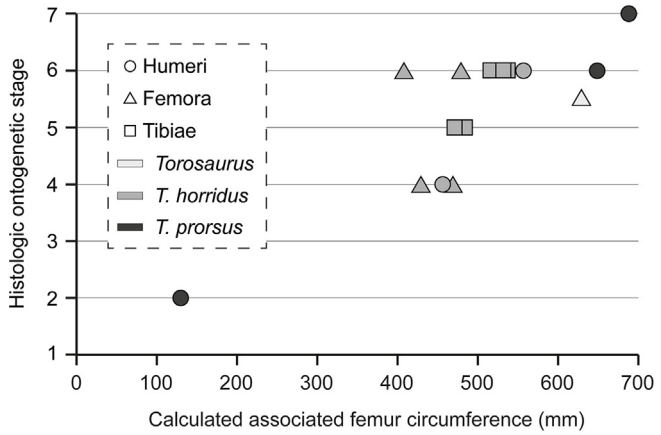

Fig. 19. Relationship between body size and HOS for *T. horridus*, *T. prorsus* and *Torosaurus*. Bone size is represented by limb bone circumference normalized to femur circumference based on ratios of the associated *Triceratops* specimen RGM.1332500. Both *T. prorsus* and *Torosaurus* do not significantly deviate from the overall correlation for *T. horridus*.

T. horridus individuals in our dataset would have grown slightly larger, reaching HOS 7 and skeletal maturity at approximately the same body size as *T. prorsus*. Overall, the presented *Triceratops* and *Torosaurus* histological database is currently too small to observe unequivocal taxonomic differences in ontogenetic growth patterns at the genus and species level. Future research focussing on the skeletal unity (i.e., potential for associated individuals (Wiersma-Weyand et al., 2021)) of the DTB *Triceratops* should provide insights into the developmental timing of cranial and postcranial skeletal maturity and will help in clarifying the taxonomic ambiguity between *Triceratops* and *Torosaurus* specifically.

5. Conclusions

Histological analyses of *Triceratops* limb bones plus auxiliary specimens revealed for the first time the growth pattern of this iconic ornithischian dinosaur. All limb bones of the stylopodium and zeugopodium show a consistent histology, with variations mainly due to cortical thickness as explained by the three-front model, and there is a clear relationship between body size and histologic ontogenetic stage. Ontogenetically young individuals — as represented by the small humerus RSM P.2691 — show a well-vascularized woven-parallel complex typical for actively growing endothermic juvenile animals and contains a mix of circumferential and longitudinal primary osteons. However, the dominant bone tissue type shifts into cycles of parallel-fibred bone and woven-fibred complex throughout ontogeny allowing to define the histological development through histologic ontogenetic stages. Subadult *Triceratops* limb bones are characterized by irregular alternating zones of thicker layers of woven and thinner layers of parallel-fibred bone tissue. Bone remodelling is only moderate, and simple vascular canals in the periosteal surface indicate active growth. As the animal approached skeletal maturity, the primary bone of adult *Triceratops* shows higher proportions of parallel-fibred bone tissue and increased bone remodelling. Skeletal maturity is indicated by an EFS near the periosteal surface.

Apart from the EFS in mature specimens, regular growth cycles are rare in the studied elements. A small number of elements preserve higher numbers of zones and annuli, but the majority of the sections show a poorly developed skeletochronological record, which we now consider typical for ceratopsid histology. Ribs and vertebrae preserve small numbers of LAGs, but the heavy remodelling combined with the significant influence of bone morphogenesis on growth mark spacing in ribs does not allow for accurate analysis of the primary growth record. Contrary to sauropod rib histology, *Triceratops* (and most likely other ceratopsids) show faster growing woven-parallel bone tissue in their ribs possibly hampering LAG deposition.

While the zones of parallel-fibred tissue in the limb bones are less vascularized than the zones of woven-parallel complex, they all contain primary osteons and form 'fibrolamellar' parallel-fibred bone (PFLC) similar to the modified laminar bone described for some sauropod taxa. In fact, *Triceratops* showed overall high vascularization throughout ontogeny across multiple different limb elements. The prevalence of parallel-fibred bone tissue relatively early in ontogeny combined with consistently high vascularisation suggests that *Triceratops* had a relatively fast and continuous growth rate, but not as rapid as is seen in many other groups of non-avian dinosaurs.

The zonation of parallel-fibred bone tissue is also observed in more basal ceratopsians but becomes more pronounced in *Triceratops*. Comparisons with other ceratopsids provide equivocal results due to lack of ontogenetically well-constrained material and warrants additional data on ceratopsid histology. Our work adds to the rather limited ceratopsian histological database, being based on the most extensive dataset for any large-bodied neoceratopsian, and is beginning to unravel the evolution of ceratopsian growth strategies.

Data availability

All data is in the original manuscript and supplementary files.

Acknowledgements

We greatly appreciated the hospitality of Nancy and Donley Darnell and their help during the many field seasons on their property. In addition, many thanks go to our entire team of colleagues and volunteers for their enthusiasm and efforts in retrieving the fossil material. Special thanks go to preparators Yasmin Grooters, Martijn Guliker and their team of volunteers (Naturalis Biodiversity Center, the Netherlands) for handling and preparing the studied material for research. Additionally, many thanks go to Natasja den Ouden (Naturalis Biodiversity Center, the Netherlands) for streamlining access to the material and handling of the destructive sampling requests. We want to express our gratitude towards John van Gulik (Canon Medical Systems, the Netherlands) and Berend Stoel (Leids Universitair Medisch Centrum, the Netherlands) for access to CT scanners and their flexibility amidst the COVID outbreak. We like to thank Olaf Dülfer (Section Paleontology, Institute of Geosciences, University of Bonn, Germany) and Bouke Lacet (Faculty of Science, Vrije Universiteit, Amsterdam, the Netherlands) for making the thin-sections used in this study. For access to additional *Triceratops* material, we like to express our sincerest gratitude to Jordan Mallon (Canadian Museum of Nature, Ottawa, Canada) and Ryan McKellar (Royal Saskatchewan Museum, Regina, Canada). The project is funded by the Dutch Research Council (NWO) through ALW Open Programme (ALWOP.633). We like to acknowledge Dylan Bastiaans (PIMUZ, Switzerland) for his valuable contributions and input in developing the initial research plan. Furthermore, our gratitude goes towards the Mondriaan Fonds for their important contribution in sponsoring the field seasons. Lastly, many thanks to the two anonymous reviewers for their valuable and insightful comments that greatly improved the manuscript.

References

Baag, S.J., Lee, Y.N., 2022. Bone histology on *Koreaceratops hwaseongensis* (Dinosauria: Ceratopsia) from the Lower Cretaceous of South Korea. Cretaceous Research 134, 105150. https://doi.org/10.1016/j.cretres.2022.105150.

Botha, J., Choiniere, J.N., Benson, R.B.J., 2022. Rapid growth preceded gigantism in sauropodomorph evolution. Current Biology 32, 4501–4507.e2. https://doi.org/10.1016/j.cub.2022.08.031.

Bastiaans, D., Trapman, T., Guliker, M., Kaskes, P., Schulp, A., 2016. Multigenerational assemblage of *Triceratops* from the Newcastle area, Wyoming, USA – An in-depth analysis of cranial and post-cranial ontogenesis. In: Farke, A.A., MacKenzie, A., Miller-Camp, J. (Eds.), Journal of Vertebrate Paleontology, Program and Abstracts, p. 94.

Bartos, T.T., Galloway, D.L., Hallberg, L.L., Dechesne, M., Diehl, S.F., Davidson, S.L., 2021. Geologic and Hydrogeologic Characteristics of the White River Formation, Lance Formation, and Fox Hills Sandstone, northern greater Denver Basin, southeastern Laramie County, Wyoming. In: U.S. Geological Survey Scientific Investigations Report 2021–5020, pp. 1–242. https://doi.org/10.3133/sir20215020.

Buffrénil, V. de, Quilhac, A., 2021. Bone tissue types: A brief account of currently used categories. In: Buffrénil, V. de, Ricqlès, A. de, Zylberberg, L., Padian, K. (Eds.), Vertebrate Skeletal Histology and Paleohistology. CRC Press, Boca Raton, pp. 147–190.

Buffrénil, V. de, Ricqlès, A. de, Zylberberg, L., Padian, K. (Eds.), 2021. Vertebrate Skeletal Histology and Paleohistology. CRC Press, Boca Raton.

Chiba, K., Ryan, M.J., Fanti, F., Loewen, M.A., Evans, D.C., 2018. New material and systematic re-evaluation of *Medusaceratops lokii* (Dinosauria, Ceratopsidae) from the Judith River Formation (Campanian, Montana). Journal of Paleontology 92, 272–288. https://doi.org/10.1017/jpa.2017.62.

Chinnery, B., 2004. Morphometric analysis of evolutionary trends in the ceratopsian postcranial skeleton. Journal of Vertebrate Paleontology 24 (3), 591–609. https://doi.org/10.1671/0272-4634(2004)024[0591:MAOETI]2.0.CO;2.

Chinsamy, A., Raath, M.A., 1992. Preparation of fossil bone for histological examination. Palaeontologia Africana 29, 39–44.

Chinsamy, A., Thomas, D.B., Tumarkin-Deratzian, A.R., Fiorillo, A.R., 2012. Hadrosaurs were perennial polar residents. The Anatomical Record 295, 610–614. https://doi.org/10.1002/ar.22428.

Cullen, T.M., Canale, J.I., Apesteguía, S., Smith, N.D., Hu, D., Makovicky, P.J., 2020. Osteohistological analyses reveal diverse strategies of theropod dinosaur body-size evolution. Proceedings of the Royal Society B 287, 20202258. https://doi.org/10.1098/rspb.2020.2258.

Cullen, T.M., Brown, C.M., Chiba, K., Brink, K.S., Makovicky, P.J., Evans, D.C., 2021. Growth variability, dimensional scaling, and the interpretation of osteohistological growth data. Biological Letters 17, 20210383. https://doi.org/10.1098/rsbl.2021.0383.

D'Emic, M.D., O'Connor, P.M., Sombathy, R.S., Cerda, I., Pascucci, T.R., Varricchio, D., Pol, D., Dave, A., Coria, R.A., Curry Rogers, K.A., 2023. Developmental strategies underlying gigantism and miniaturization in non-avialan theropod dinosaurs. Science 379, 811–814. https://doi.org/10.1126/science.adc8714.

Erickson, G.M., 2014. On dinosaur growth. Annual Review of Earth and Planetary Sciences 42, 675–697. https://doi.org/10.1146/annurev-earth-060313-054858.

Erickson, G.M., Druckenmiller, P.S., 2011. Longevity and growth rate estimates for a polar dinosaur: a *Pachyrhinosaurus* (Dinosauria: Neoceratopsia) specimen from the North Slope of Alaska showing a complete developmental record. Historical Biology 23, 327–334. https://doi.org/10.1080/08912963.2010.546856.

Erickson, G.M., Tumanova, T.A., 2000. Growth curve of *Psittacosaurus mongoliensis* Osborn (Ceratopsia: Psittacosauridae) inferred from long bone histology. Zoological Journal of the Linnean Society 130, 551–566. https://doi.org/10.1111/j.1096-3642.2000.tb02201.x.

Forster, C.A., 1996a. New information on the skull of *Triceratops*. Journal of Vertebrate Paleontology 16 (2), 246–258. https://doi.org/10.1080/02724634.1996.10011312.

Forster, C.A., 1996b. Species resolution in *Triceratops*: Cladistic and morphometric approaches. Journal of Vertebrate Paleontology 16 (2), 259–270. https://doi.org/10.1080/02724634.1996.10011313.

Fostowicz-Frelik, L., Słowiak, J., 2018. Bone histology of *Protoceratops andrewsi* from the Late Cretaceous of Mongolia and its biological implications. Acta Palaeontologica Polonica 63, 503–517. https://doi.org/10.4202/app.00463.2018.

Goldsmith, E.R., 2018. Bone histology and geochemical taphonomy of Arctic centrosaurine ceratopsids from the Kikak-Tegoseak Quarry (North Slope, Alaska) (Unpubl. MSc thesis) Temple University, Philadelphia, 154 pp.

Goodwin, M.B., Clemens, W.A., Horner, J.R., Padian, K., 2006. The smallest known *Triceratops* skull: new observations on ceratopsid cranial anatomy and ontogeny. Journal of Vertebrate Paleontology 26, 103–112. https://doi.org/10.1671/0272-4634(2006)26[103:TSKTSN]2.0.CO;2.

Hedrick, B.P., Goldsmith, E., Rivera-Sylva, H., Fiorillo, A.R., Tumarkin-Deratzian, A.R., Dodson, P., 2020. Filling in gaps in the ceratopsid histologic database: histology of two basal centrosaurines and an assessment of the utility of rib histology in the Ceratopsidae. The Anatomical Record 303, 935–948. https://doi.org/10.1002/ar.24099.

Henderson, D.M., 2014. In: Duck soup: the floating fates of hadrosaurs and ceratopsians at Dinosaur Provincial Park. In: Eberth, D.A., Evans, D.C. (Eds). Hadrosaurs. Indiana University Press, Bloomington, pp. 459–466.

Holmes, R., Ryan, M.J., 2013. The postcranial skeleton of *Styracosaurus albertensis*. Kirtlandia 58, 5–37.

Horner, J.R., Ricqlès, A. de, Padian, K., 1999. Variation in dinosaur skeletochronology indicators: implications for age assessment and physiology. Paleobiology 25, 295–304. https://doi.org/10.1017/S0094837300021308.

Horner, J.R., Ricqlès, A. de, Padian, K., 2000. Long bone histology of the hadrosaurid dinosaur *Maiasaura peeblesorum*: growth dynamics and physiology based on an ontogenetic series of skeletal elements. Journal of Vertebrate Paleontology 20, 115–129. https://doi.org/10.1671/0272-4634(2000)020[0115:LBHOTH]2.0.CO;2.

Horner, J.R., Goodwin, M.B., 2006. Major cranial changes during *Triceratops* ontogeny. Proceedings of the Royal Society B 273, 2757–2761. https://doi.org/10.1098/rspb.2006.3643.

Horner, J.R., Goodwin, M.B., 2008. Ontogeny of cranial epi-ossifications in *Triceratops*. Journal of Vertebrate Paleontology 28, 134–144. https://doi.org/10.1671/0272-4634(2008)28[134:OOCEIT]2.0.CO;2.

Horner, J.R., Lamm, E.T., 2011. Ontogeny of the parietal frill of *Triceratops*: A preliminary histological analysis. Comptes Rendus Palevol 10, 439–452. https://doi.org/10.1016/j.crpv.2011.04.006.

Horner, J.R., Padian, K., 2004. Age and growth dynamics of *Tyrannosaurus rex*. Proceedings of the Royal Society B 271, 1875–1880. https://doi.org/10.1098/rspb.2004.2829.

Kaskes, P., Bastiaans, D., Verhage, O., de Rooij, J., Guliker, M., Schulp, A.S., 2019. Taphonomy of a unique multigenerational *Triceratops* bonebed from eastern Wyoming (USA): new insights from a multi-proxy perspective. In: Godefroit, P., Stein, K., Smith, T., Lambert, O., Olive, S. (Eds.), Program and Abstracts, European Association of Vertebrate Palaeontologists: XVII Annual Meeting, Brussels, Belgium, 2/07/19, vol. 17, p. 54.

Klein, N., Sander, M., 2008. Ontogenetic stages in the long bone histology of sauropod dinosaurs. Paleobiology 34, 247–263. https://doi.org/10.1666/0094-8373(2008)034[0247:OSITLB]2.0.CO;2.

Klein, N., Sander, P.M., Stein, K., Le Loeuff, J., Carballido, J.L., Buffetaut, E., 2012. Modified laminar bone in *Ampelosaurus atacis* and other titanosaurs (Sauropoda): Implications for life history and physiology. PLoS One 7, e36907. https://doi.org/10.1371/journal.pone.0036907.

Lamm, E.T., 2013. Preparation and sectioning of specimens. In: Padian, K., Lamm, E.T. (Eds.), Bone Histology of Fossil Tetrapods: Advancing Methods, Analysis, and Interpretation. University of California Press, Berkeley, pp. 55–160.

Lee, A., 2007. Bone microstructure reflects evolution of large size in horned dinosaurs. Microscopy and Microanalysis 13, 502–503. https://doi.org/10.1017/S1431927607078658.

Lee, Y.N., Ryan, M.J., Kobayashi, Y., 2011. The first ceratopsian dinosaur from South Korea. Naturwissenschaften 98, 39–49. https://doi.org/10.1007/s00114-010-0739-y.

Levitt, C.G., 2013. Bone histology and growth of chasmosaurine ceratopsid dinosaurs from the Late Campanian Kaiparowits Formation, southern Utah (Unpubl. MSc Thesis). The University of, Utah, Salt Lake City, p. 149.

Longrich, N.R., Field, D.J., 2012. *Torosaurus* is not *Triceratops*: Ontogeny in chasmosaurine ceratopsids as a case study in dinosaur taxonomy. PLoS One 7, e32623. https://doi.org/10.1371/journal.pone.0032623.

Maidment, S.C.R., Barrett, P.M., 2011. A new specimen of *Chasmosaurus belli* (Ornithischia: Ceratopsidae), a revision of the genus, and the utility of postcrania in the taxonomy and systematics of ceratopsid dinosaurs. Zootaxa 2963, 1. https://doi.org/10.11646/zootaxa.2963.1.1.

Maiorino, L., Farke, A.A., Kotsakis, T., Piras, P., 2013. Is *Torosaurus Triceratops*? Geometric morphometric evidence of Late Maastrichtian ceratopsid dinosaurs. PLoS One 8, e81608. https://doi.org/10.1371/journal.pone.0081608.

Mallon, J.C., Ott, C.J., Larson, P.L., Iuliano, E.M., Evans, D.C., 2016. *Spiclypeus shipporum* gen. et sp. nov., a boldly audacious new chasmosaurine ceratopsid (Dinosauria: Ornithischia) from the Judith River Formation (Upper Cretaceous: Campanian) of Montana, USA. PLoS One 11, e0154218. https://doi.org/10.1371/journal.pone.0154218.

Mallon, J.C., Holmes, R., 2010. Description of a complete and fully articulated chasmosaurine postcranium previously assigned to *Anchiceratops* (Dinosauria: Ceratopsia). In: Ryan, M.J., Chinnery-Allgeier, B.J., Eberth, D.A. (Eds.), New Perspectives on Horned Dinosaurs. The Royal Tyrrell Museum Ceratopsian Symposium. Indiana University Press, Bloomington, pp. 189–202.

Mallon, J.C., Holmes, R.B., Bamforth, E.L., Schumann, D., 2022. The record of *Torosaurus* (Ornithischia: Ceratopsidae) in Canada and its taxonomic implications. Zoological Journal of the Linnean Society 195, 157–171. https://doi.org/10.1093/zoolinnean/zlab120.

Margerie, E. de, Cubo, J., Castanet, J., 2002. Bone typology and growth rate: testing and quantifying 'Amprino's rule' in the mallard (*Anas platyrhynchos*). Comptes Rendus Biologies 325, 221–230. https://doi.org/10.1016/S1631-0691(02)01429-4.

Margerie, E. de, Robin, J.-P., Verrier, D., Cubo, J., Groscolas, R., Castanet, J., 2004. Assessing a relationship between bone microstructure and growth rate: a fluorescent labelling study in the king penguin chick (*Aptenodytes patagonicus*). Journal of Experimental Biology 207, 869–879. https://doi.org/10.1242/jeb.00841.

Mitchell, J., Sander, P.M., 2014. The three-front model: a developmental explanation of long bone diaphyseal histology of Sauropoda. Biological Journal of the Linnean Society 112, 765–781. https://doi.org/10.1111/bij.12324.

Mitchell, J., Sander, P.M., Stein, K., 2017. Can secondary osteons be used as ontogenetic indicators in sauropods? Extending the histological ontogenetic stages

into senescence. Paleobiology 43, 321–342. https://doi.org/10.1017/pab.2016.47.
Prondvai, E., Godefroit, P., Adriaens, D., Hu, D.-Y., 2018. Intraskeletal histovariability, allometric growth patterns, and their functional implications in bird-like dinosaurs. Scientific Reports 8, 258. https://doi.org/10.1038/s41598-017-18218-9.
Redelstorff, R., Sander, P.M., 2009. Long and girdle bone histology of *Stegosaurus* : implications for growth and life history. Journal of Vertebrate Paleontology 29, 1087–1099. https://doi.org/10.1671/039.029.0420.
Redelstorff, R., Hübner, T.R., Chinsamy, A., Sander, P.M., 2013. Bone histology of the stegosaur *Kentrosaurus aethiopicus* (Ornithischia: Thyreophora) from the Upper Jurassic of Tanzania. The Anatomical Record 296, 933–952. https://doi.org/10.1002/ar.22701.
Reizner, J.A., 2010. An ontogenetic series and population histology of the ceratopsid dinosaur *Einiosaurus procurvicornis* (Unpubl. MSc Thesis).. Montana State University, Bozeman, pp. 97.
Rooij, J. de, 2018. Discovery of a *Triceratops* bonebed: *Triceratops* long bone histology and implications on social behaviour (Unpubl. MSc thesis) Utrecht University, Utrecht, pp. 71.
Rooij, J. de, van der Lubbe, J.H.J.L., Verdegaal, S., Hulscher, M., Tooms, D., Kaskes, P., Verhage, O., Portanger, L., Schulp, A.S., 2022. Stable isotope record of *Triceratops* from a mass accumulation (Lance Formation, Wyoming, USA) provides insights into *Triceratops* behaviour and ecology. Palaeogeography, Palaeoclimatology, Palaeoecology 607, 111274. https://doi.org/10.1016/j.palaeo.2022.111274.
Sampson, S.D., Loewen, M.A., 2010. Unraveling a radiation: a review of the diversity, stratigraphic distribution, biogeography, and evolution of horned dinosaurs (Ornithischia: Ceratopsidae). In: Ryan, M.J. Chinnery-Allgeier, B.J. Eberth, D.A. New Perspectives on Horned Dinosaurs: The Royal Tyrrell Museum Ceratopsian Symposium. Indiana University Press, Bloomington, pp. 405–427.
Sander, P.M., 2000. Longbone histology of the Tendaguru sauropods: implications for growth and biology. Paleobiology 26, 466–488. https://doi.org/10.1666/0094-8373(2000)026<0466:LHOTTS>2.0.CO;2.
Sander, P.M., Wintrich, T., 2021. Sauropterygia: Histology of Plesiosauria. In: Buffrénil, V. de, Ricqlès, A. de, Zylberberg, L., Padian, K. (Eds.), Vertebrate Skeletal Histology and Paleohistology, CRC Press, Boca Raton, pp. 444–457.
Scannella, J.B., Horner, J.R., 2010. *Torosaurus* Marsh, 1891, is *Triceratops* Marsh, 1889 (Ceratopsidae: Chasmosaurinae): synonymy through ontogeny. Journal of Vertebrate Paleontology 30, 1157–1168. https://doi.org/10.1080/02724634.2010.483632.
Scannella, J.B., Horner, J.R., 2011. '*Nedoceratops*': An example of a transitional morphology. PLoS One 6, e28705. https://doi.org/10.1371/journal.pone.0028705.
Sander, P.M., Klein, N., Stein, K., Wings, O., 2011. Sauropod bone histology and its implications for sauropod biology. In: Klein, N., Remes, C., Gee, C.T., Sander, P.M. (Eds.), Biology of the Sauropod Dinosaurs: Understanding the Life of Giants. Indiana University Press, Bloomington, pp. 276–302.
Scannella, J.B., Fowler, D.W., Goodwin, M.B., Horner, J.R., 2014. Evolutionary trends in *Triceratops* from the Hell Creek formation, Montana. Proceedings of the National Academy of Sciences of the United States of America 111 (28), 10245–10250. https://doi.org/10.1073/pnas.1313334111.
Scott, S.H.W., Ryan, M.J., Evans, D.C., 2023. Postcranial description of *Wendiceratops pinhornensis* and a taphonomic analysis of the oldest monodominant ceratopsid bonebed. The Anatomical Record 306, 1824–1841. https://doi.org/10.1002/ar.25045.
Sereno, P.C., 2010. Taxonomy, cranial morphology, and relationships of parrot-beaked dinosaurs (Ceratopsia: *Psittacosaurus*). In: Ryan, M.J., Chinnery-Allgeier, B.J., Eberth, D.A. (Eds.), New Perspectives on Horned Dinosaurs: The Royal Tyrrell Museum Ceratopsian Symposium, Indiana University Press, Bloomington, pp. 21–58.
Skutschas, P., Morozov, S., Averianov, A., Leshchinskiy, S., Ivantsov, S., Fayngerts, A., Feofanova, O., Vladimirova, O., Slobodin, D., 2021. Femoral histology and growth patterns of the ceratopsian dinosaur *Psittacosaurus sibiricus* from the Early Cretaceous of Western Siberia. Acta Palaeontologica Polonica 66, 437–447. https://doi.org/10.4202/app.00819.2020.
Słowiak, J., Szczygielski, T., Ginter, M., Fostowicz-Frelik, Ł., 2020. Uninterrupted growth in a non-polar hadrosaur explains the gigantism among duck-billed dinosaurs. Palaeontology 63, 579–599. https://doi.org/10.1111/pala.12473.
Stein, K., Sander, P.M., 2009. Histological core drilling: a less destructive method for studying bone histology. In: Brown, M.A., Kane, J.F., Parker, W.G. (Eds.), Methods in Fossil Preparation: Proceedings of the First Annual Fossil Preparation and Collections Symposium, pp. 69–80.
Stein, K., Csiki, Z., Rogers, K.C., Weishampel, D.B., Redelstorff, R., Carballido, J.L., Sander, P.M., 2010. Small body size and extreme cortical bone remodeling indicate phyletic dwarfism in *Magyarosaurus dacus* (Sauropoda: Titanosauria). Proceedings of the National Academy of Sciences of the United States of America 107, 9258–9263. https://doi.org/10.1073/pnas.1000781107.
Stein, M., Hayashi, S., Sander, P.M., 2013. Long bone histology and growth patterns in ankylosaurs: Implications for life history and evolution. PLoS One 8, e68590. https://doi.org/10.1371/journal.pone.0068590.
Sues, H.D., Averianov, A., 2009. *Turanoceratops tardabilis*—the first ceratopsid dinosaur from Asia. Naturwissenschaften 96, 645–652. https://doi.org/10.1007/s00114-009-0518-9.
Tokaryk, T.T., 1986. Ceratopsian dinosaurs from the Frenchman Formation (Upper Cretaceous) of Saskatchewan. Canadian Field-Naturalist 100 (2), 192–196.
Vice, R.M., 2020. The forelimb and pectoral girdle of *Pachyrhinosaurus lakustai* (Ceratopsia, Centrosaurinae) (Unpubl. MSc Thesis). University of Alberta, Alberta, p. 162.
Waskow, K., 2019. Patterns of life history recorded in the dorsal rib histology of amniotes. (PhD dissertation)., University of Bonn, Bonn.
Waskow, K., Mateus, O., 2017. Dorsal rib histology of dinosaurs and a crocodylomorph from western Portugal: Skeletochronological implications on age determination and life history traits. Comptes Rendus Palevol 16, 425–439. https://doi.org/10.1016/j.crpv.2017.01.003.
Waskow, K., Sander, P.M., 2014. Growth record and histological variation in the dorsal ribs of *Camarasaurus* sp. (Sauropoda). Journal of Vertebrate Paleontology 34, 852–869. https://doi.org/10.1080/02724634.2014.840645.
Wiersma-Weyand, K., Canoville, A., Siber, H.-J., Sander, P.M., 2021. Testing hypothesis of skeletal unity using bone histology: The case of the sauropod remains from the Howe-Stephens and Howe Scott quarries (Morrison Formation, Wyoming, USA). Palaeontologia Electronica 24 (1), a10. https://doi.org/10.26879/766.
Wolfe, D.G., Kirkland, J.I., Smith, D., Poole, K., Chinnery-Allgeier, B., McDonald, A., 2007. *Zuniceratops christopheri*: An update on the North American ceratopsid sister taxon, Zuni Basin, west-central New Mexico. In: Braman, D.R., Brinkman, D. (Eds.), Ceratopsian Symposium: Short Papers, Abstracts, and Programs. Royal Tyrell Museum of Paleontology, Drumheller, pp. 159–167.
Woodward, H.N., Horner, J.R., Farlow, J.O., 2014. Quantification of intraskeletal histovariability in *Alligator mississippiensis* and implications for vertebrate osteohistology. PeerJ 2, e422. https://doi.org/10.7717/peerj.422.
Woodward, H.N., Tremaine, K., Williams, S.A., Zanno, L.E., Horner, J.R., Myhrvold, N., 2020. Growing up *Tyrannosaurus rex*: Osteohistology refutes the pygmy "*Nanotyrannus*" and supports ontogenetic niche partitioning in juvenile *Tyrannosaurus*. Science Advances 6, eaax6250. https://doi.org/10.1126/sciadv.aax6250.
Zhao, Q., Benton, M., Hayashi, S., Xu, X., 2019. Ontogenetic stages of ceratopsian dinosaur *Psittacosaurus* in bone histology. Acta Palaeontologica Polonica 64, 323–334. https://doi.org/10.4202/app.00559.2018.
Zheng, W., Jin, X., Xu, X., 2015. A psittacosaurid-like basal neoceratopsian from the Upper Cretaceous of central China and its implications for basal ceratopsian evolution. Scientific Reports 5, 14190. https://doi.org/10.1038/srep14190.

Appendix A. Supplementary data

Supplementary data to this article can be found online at https://doi.org/10.1016/j.cretres.2023.105738.